(4)

AFGL-TR-89-0034

AD-A208 276

P_n From the Nevada Test Site

L. J. Burdick
C. K. Saikia
N. F. Smith

Woodward-Clyde Consultants
566 El Dorado Street
Suite 100
Pasadena, CA 91101

15 December 1988

Scientific Report No. 3

APPROVED FOR PUBLIC RELEASE; DISTRIBUTION UNLIMITED

AIR FORCE GEOPHYSICS LABORATORY
AIR FORCE SYSTEMS COMMAND
UNITED STATES AIR FORCE
HANSCOM AIR FORCE BASE, MASSACHUSETTS 01731-5000

Sponsored by: Defense Advanced Research Projects Agency
Nuclear Monitoring Research Office
DARPA Order No. 5307
Monitored by: Air Force Geophysics Laboratory
Contract No. F19628-87-C-0081

The views and conclusions contained in this document are those of the authors and should not be interpreted as representing the official policies, either expressed or implied, of the Defense Advanced Research Projects Agency or the US Government.

"This technical report has been reviewed and is approved for publication"

JAMES F. LEWKOWICZ
Contract Manager
Solid Earth Geophysics Branch
Earth Sciences Division

JAMES C. BATTIS
Acting Chief
Solid Earth Geophysics Branch
Earth Sciences Division

FOR THE COMMANDER

DONALD H. ECKHARDT, Director
Earth Sciences Division

This document has been reviewed by the ESD Public Affairs Office (PA) and is releasable to the National Technical Information Service (NTIS).

Qualified requestors may obtain additional copies from the Defense Technical Information Center. All others should apply to the National Technical Information Service.

If your address has changed, or if you wish to be removed from the mailing list, or if the addressee is no longer employed by your organization, please notify AFGL/DAA, Hanscom AFB, MA 01731-5000. This will assist us in maintaining a current mailing list.

Do not return copies of this report unless contractual obligations or notices on a specific document requires that it be returned.

REPORT DOCUMENTATION PAGE

1a REPORT SECURITY CLASSIFICATION Unclassified	1b RESTRICTIVE MARKINGS
2a SECURITY CLASSIFICATION AUTHORITY	3 DISTRIBUTION/AVAILABILITY OF REPORT Approved for public release; Distribution unlimited.
2b DECLASSIFICATION/DOWNGRADING SCHEDULE	
4 PERFORMING ORGANIZATION REPORT NUMBER(S) WCCP-R-88-03	5 MONITORING ORGANIZATION REPORT NUMBER(S) AFGL-TR-89-0034
6a NAME OF PERFORMING ORGANIZATION Woodward-Clyde Consultants 6b OFFICE SYMBOL (If applicable)	7a NAME OF MONITORING ORGANIZATION Air Force Geophysics Laboratory
6c ADDRESS (City, State, and ZIP Code) 566 El Dorado Street, Suite 100 Pasadena, CA 91101	7b ADDRESS (City, State, and ZIP Code) Hanscom Air Force Base Massassachusetts, 01731-5000
8a NAME OF FUNDING/SPONSORING ORGANIZATION DARPA 8b OFFICE SYMBOL (If applicable)	9 PROCUREMENT INSTRUMENT IDENTIFICATION NUMBER F19628-87-C-0081
8c ADDRESS (City, State, and ZIP Code) 1400 Wilson Boulevard Arlington, VA 22209	10 SOURCE OF FUNDING NUMBERS PROGRAM ELEMENT NO: 62714E; PROJECT NO: 7A10; TASK NO: DA; WORK UNIT ACCESSION NO: DD
11 TITLE (Include Security Classification) P_n from the Nevada Test Site	
12 PERSONAL AUTHOR(S) L. J. Burdick, C. K. Saikia, N. F. Smith	
13a TYPE OF REPORT Scientific No. 3 13b TIME COVERED FROM 3/5/88 TO 9/5/88	14 DATE OF REPORT (Year, Month, Day) 1988 December 15 15 PAGE COUNT 80
16 SUPPLEMENTARY NOTATION	
17 COSATI CODES FIELD / GROUP / SUB-GROUP	18 SUBJECT TERMS (Continue on reverse if necessary and identify by block number) Regional Discriminates, P_n, P_g, Synthetic Seismograms.
19 ABSTRACT (Continue on reverse if necessary and identify by block number) (See next page)	
20 DISTRIBUTION/AVAILABILITY OF ABSTRACT ☒ UNCLASSIFIED/UNLIMITED ☐ SAME AS RPT ☐ DTIC USERS	21 ABSTRACT SECURITY CLASSIFICATION Unclassified
22a NAME OF RESPONSIBLE INDIVIDUAL James F. Lewkowicz	22b TELEPHONE (Include Area Code) (617) 377-3028 22c OFFICE SYMBOL AFGL/LWH

DD FORM 1473, 84 MAR 83 APR edition may be used until exhausted
All other editions are obsolete

SECURITY CLASSIFICATION OF THIS PAGE
Unclassified

ABSTRACT

A regional event discriminant is being developed and tested based on the waveform of high frequency P_n. The data base being used in the development consists of signals from explosions and earthquakes recorded on the western U.S. digital network. This net consists of the four LLNL stations MNV, KNB, ELK and LAC; the two DWWSSN stations ALQ and JAS and the two university run stations PFO and PAS. It has been discovered that at most stations the waveform of P_n onset is remarkably stable and different from the corresponding waveforms from earthquakes. A forward modeling study of broad band explosion P_n's revealed that the distinctive character of their waveform is caused by a strong pP_n arrival. Depth phases from earthquakes arrive much later in the signal. It was found that a clear effective pP_n arrival was present in all cases. However, it consistently arrives later than the predicted elastic time. For Pahute events, the amplitude of effective pP is close to the elastic predictions. For Yucca Valley, it is consistently larger indicating the effect of a site dependent nonlinear process in the source region. An appropriate value of t^* for P_n appears to be in the range of 0.1 to 0.2 seconds. The frequency content of the explosion P_n energy indicates that it is caused by turning rays in the lid gradient rather than true head waves traveling on the crust mantle interface. The discrimination capacity of the P_n waveform was measured quantitatively by correlating the average explosion P_n trace with a data base of explosion and earthquake signals. The populations separated to a significant level down to magnitudes less than 4.0. It was found that the average explosion waveform from one station could be used to discriminate data from a different station establishing that the P_n waveform discriminant is transportable.

TABLE OF CONTENTS

INTRODUCTION

High frequency regional data appears to be among the most unstable and difficult to characterize in seismology. For this reason, most of the attempts to solve the regional discrimination problem have been based on highly empirical approaches. Ratios of phase amplitudes in either the time or frequency domain have been tested to find whether they are systematically different for earthquakes and explosions. Recently, Taylor et al. (1988) have demonstrated an impressive capability for event discrimination using spectral ratios of Lg. In essence, they demonstrated that regional signals from explosions are systematically lower in frequency content than earthquakes. This confirms an earlier result of Murphy and Bennett (1982). Though development of this discriminant represents a significant advance, there remain important questions of the transportability of the method. The reason is that a deterministic model for the change of spectral behavior between earthquake and explosion sources is not available. There is no evidence in teleseismic data that explosion sources have a different spectral decay rate than earthquakes. Most investigators assume that both sources fall off as f^{-2}, though Burger et al. (1987) have shown that this is not necessarily true. Studies which have indicated that explosions are actually enriched in high frequency with respect to earthquakes include those of Savino et al. (1980), Everendon et al. (1986) and von Seggern and Rivers (1979). Thus, if the spectral discriminant works consistently on Lg in the western United States, it must be related to phenomena associated with Lg propagation there. We can not rely on the same processes to occur in a consistent fashion in other regions.

To avoid such difficulties in transporting discriminants to new tectonic and seismic regimes, it will be necessary to develop discriminants based on a sound understanding of the physical processes which underlie them. This knowledge will permit an assessment of whether and how the discriminant should be modified

for other areas. The investigations discussed here are directed at establishing what the most stable portions of the regional P wave signal are, and if they can be modeled in a deterministic fashion. Specifically, we will discuss observations of NTS nuclear events at stations in the western U.S. digital network. We have used arrays of events to form seismic sections at each station and examined them for stable arrivals. Most of the P_n and P_g wave trains exhibit a low level of coherence. However, we have found that the very onset of P_n is remarkably stable at high frequency and that it has a character strongly influenced by free surface phases. Since free surface phases occur later for earthquakes than explosions, it is possible to develop a discriminant based on P_n onset. Because the physics behind the discriminant is straightforward, transporting the technique to other regions should not pose a significant problem.

For the purposes of this discussion, we will define the western U. S. digital array as including the four LLNL stations MNV, KNB, LAC and ELK; the two DWWSSN stations ALQ and JAS and the Caltech and UCSD stations, PAS and PFO. In the following report, we will discuss the seismic sections of the regional P wave train we have assembled for each station to date. We will compare the relative coherency of P_n and P_g, and determine the average P_n onset waveform by stacking. We will identify stations with complex receiver functions and those being affected by complex structure in the lithosphere. This structure explains some of the instability of the ratio of the amplitude of the P_n and P_g arrivals. We will then present modeling studies of the observed P_n onset waveforms which delineate the effects of pP. We will also model some of the clear effects of source scaling. Finally, we will demonstrate how P_n onset can be used to discriminate explosions from earthquakes.

THE WESTERN U.S. DIGITAL ARRAY

The short period instruments at the two DWWSSN stations are relatively band limited in that they are designed to mimic the short period Benioffs of the old WWSSN. The rest of the stations have modern broad band instruments. To make the following comparisons uniform, we have converted all of the data to the short period WWSSN response. In later sections, we will consider deconvolved broad band data. Figure 1 is a map displaying the stations of the digital array as they distribute about NTS. Azimuthal coverage is relatively good, and stations LAC and PFO are almost exactly aligned with NTS. Shown as circles are the locations of earthquakes we have used for discrimination studies. The closest station is MNV at a range of 195 km to the nearest NTS events and the farthest is ALQ at 890 km. The other stations are at about 325 to 375 km in range on average.

MNV The first station in the array we wish to discuss is Mina, Nevada. As shown in Figure 1, it is located northwest of the test site. Figure 2 shows the vertical component observations of 4 Pahute events at that station. In this and all of the following, seismic sections are shown reduced to the apparent velocity of P_n; that is the arrival time is selected manually and a ten second leader is added to it. The P_n barely emerges from the front of the P_g, but it has a stable form which we will show in the following to be very significant. This shape can be seen most clearly in the bottom trace. The P_n arrival has a small upswing first which we will refer to as the "a" swing. This is followed by a strong "b" swing downward and a structured "c" swing upward. The "c" swing exhibits a double shoulder or splitting. In the following, we will show that this feature is caused by the arrival of pP_n.

Western U.S. Digital Network

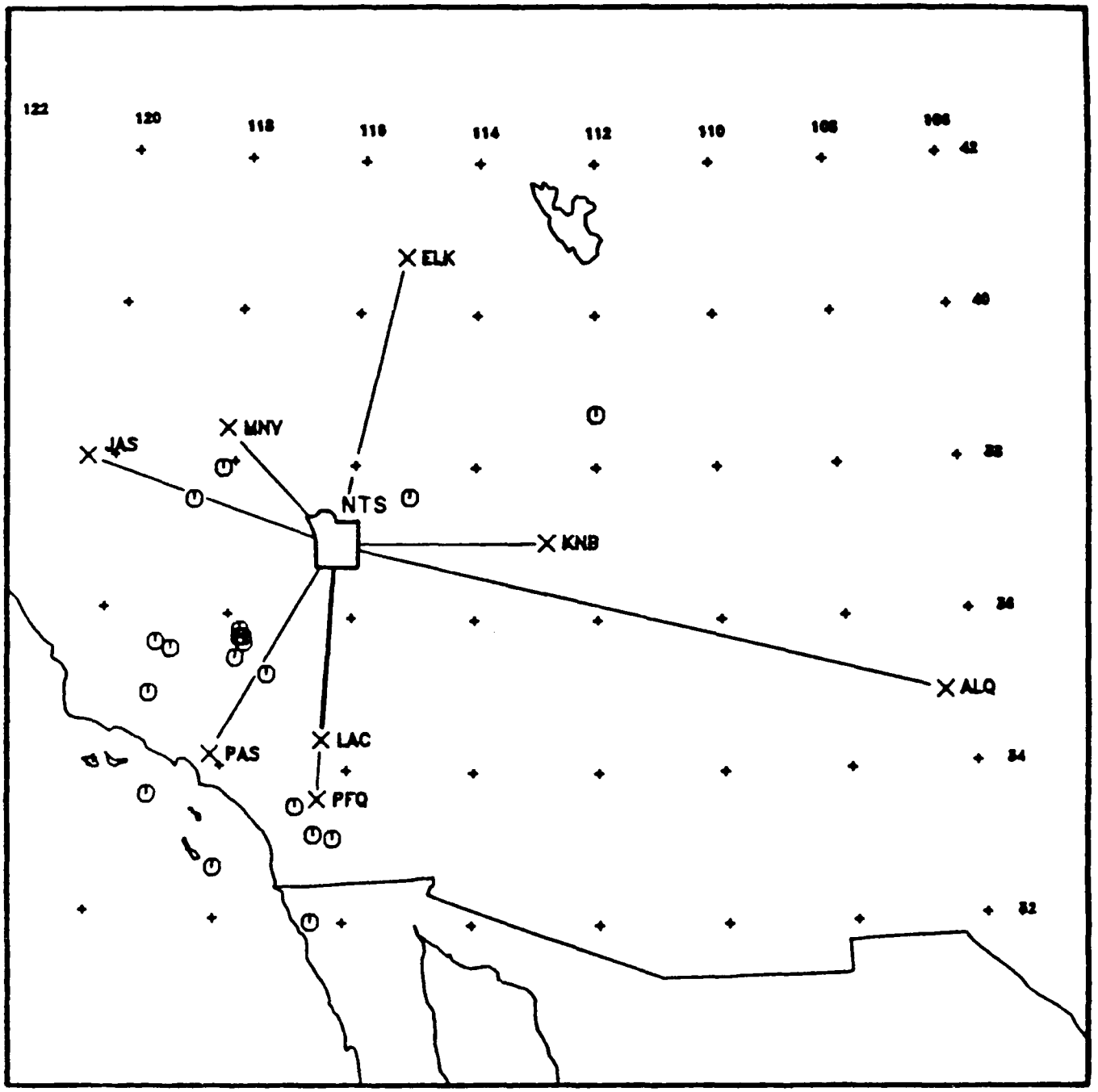

Figure 1. The western United States digital array as defined for the purposes of this study. MNV, KNB, LAC and ELK are LLNL stations. ALQ and JAS are DWWSSN stations and PAS and PFO are university run stations. The open circles are the locations of earthquakes in the discrimination data base.

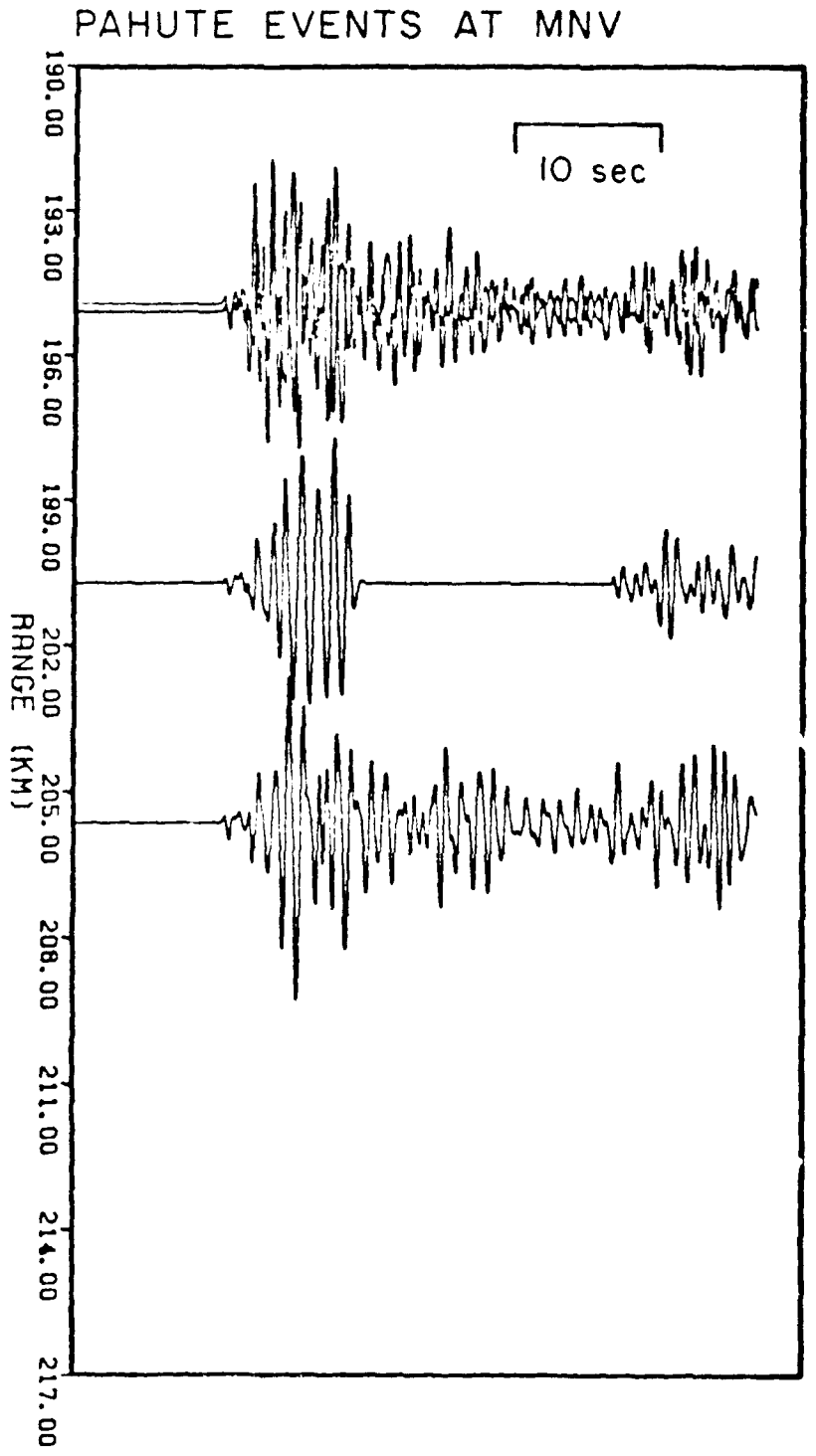

Figure 2. A seismic section of four Pahute explosions observed at MNV. The P_n is the small signal consisting of only 3 or 4 swings ahead of the much larger P_g. The P_n waveform is stable whereas no portion of the P_g is.

The P_g arrival is as unstable in character as most high frequency regional signals usually are. There may be some periodic sequence of pulses contributing to the upper traces which could be caused by crustal resonance phases. In a previous report, we associated such phases with successive reverberations of energy in the crustal wave guide (Burdick et al., 1988). At any rate, it is clear that there is no feature in the regional P wave signal as stable as the shape of the P wave onset. It is important to note here that the relative amplitude of P_g to P_n is about 5 to 1 for the purposes of the following discussion.

Figure 3 shows a comparable section of signals from Yucca Valley events. The Pahute events are at an average of about 200 km in range, and the Yucca events are at about 231 km. Thus we see some significant P_n move out from P_g. The splitting of the c swing is apparent in all traces, particularly the bottom ones. The top two traces show a very deep split, but given that this is high frequency data the shape of P_n onset is very stable. The P_g shows no stable features in this format. No separate phases can be discerned moving through the section except for a crustal S wave at the very back. It is interesting to note that much more S is generated at Yucca Valley than at Pahute Mesa. Presumably, this is due to the stronger scattering at Yucca Valley.

We now begin to illustrate how the stable character of P_n onset can be used to develop a discrimination algorithm. The first step involves measuring the average P_n waveshape. To accomplish this we simply stack 4 to 6 observations for each station and test site This process is illustrated for MNV and Yucca Valley events in Figure 4. We particularly select records which show the split swing clearly since this feature is caused by pP, and we wish to design our discriminant to detect it. It is interesting to note the stability of the feature with respect to event size. The largest event on top is more than 2 full magnitude units larger than the smallest, yet the difference in the character of the "c"

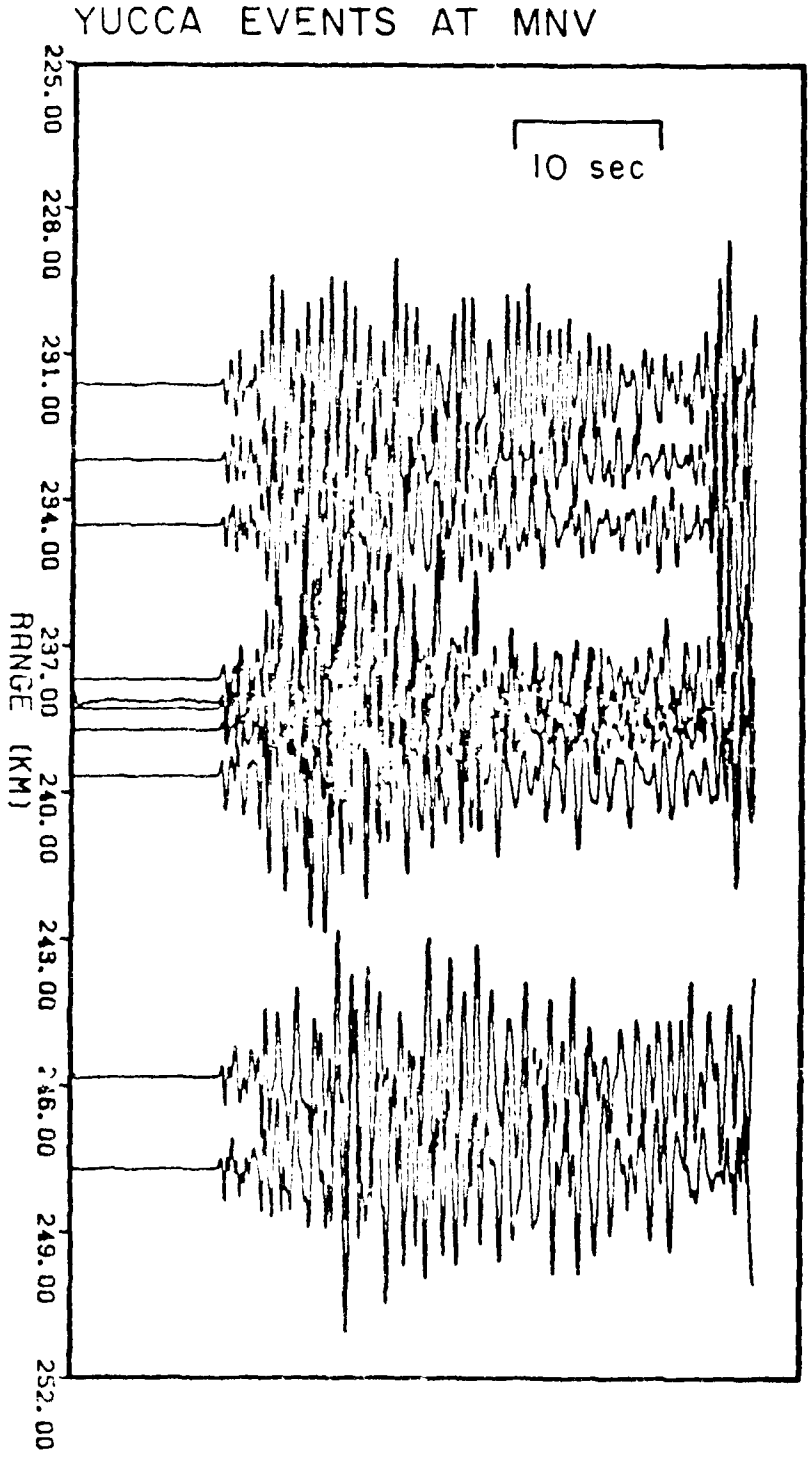

Figure 3. A seismic section of ten Yucca Valley explosions observed at MNV. The P_n wave has moved farther ahead of P_g than in the Pahute records in Figure 2. The P_n waveform is still the most stable portion of the P coda.

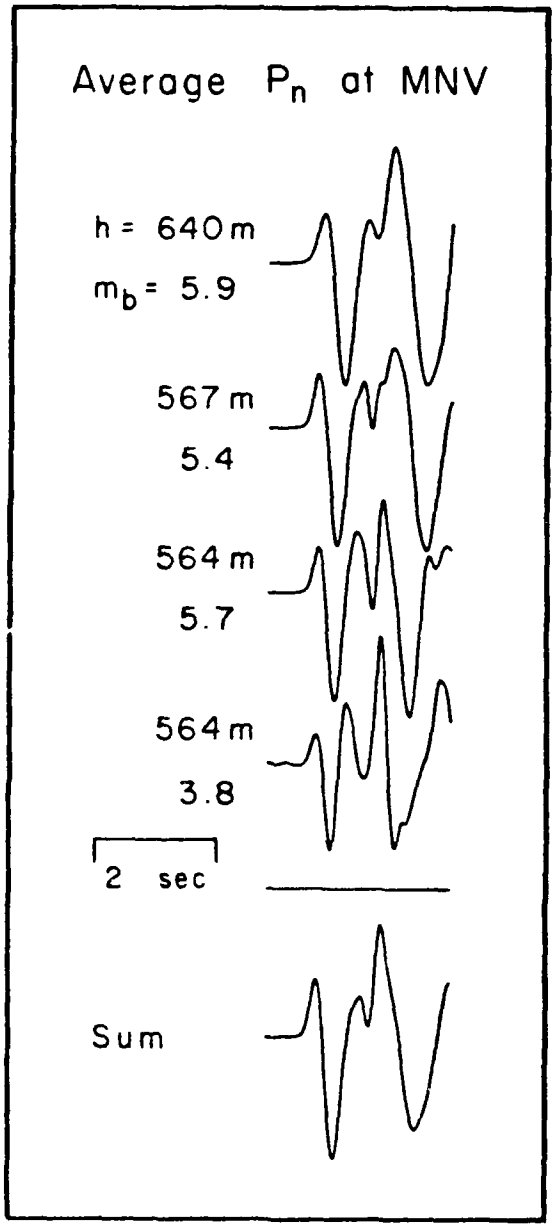

Figure 4. An illustration of the procedure of obtaining the average P_n waveform, in this instance at MNV. Four to six waveforms which exhibit the split "c" swing are selected, aligned in time and summed.

swing is minimal. The source scaling effect is obvious in that the smallest event is shorter in period than the largest. It is also worth noting that all events shown are deep, so the effect of burial depth on pP character is not apparent. We have developed average P_n waveforms like the one at the bottom of Figure 4 for all stations and test sites where it seemed appropriate, but we will not present the details of the averaging on a station by station basis. We will summarize the results at the end of this section.

KNB All of the data collected and analyzed so far are shown in seismic sections in Appendix 1. We will discuss these sections qualitatively for the next several stations to make a few key points. The first station will be Kanab, Utah. At this site the structure of the P_n onset for Pahute events strongly resembles that obtained in Figure 4 by averaging the MNV signals. The P_g signals are, on the other hand, completely different between the two stations. At KNB, the P_g appears to be dominated by a single pulse. At MNV there appeared to be several pulses for Pahute sources (see Figure 2). The physics of P_g propagation has changed in a major way in the two different azimuths. It will therefore be difficult to develop a model to explain how a discriminant based on P_g is working, and its transportability will be difficult to establish. Again there are no other phases visible in the section except P_n and P_g. Note that the ratio of the two phases is again about 5 to 1.

The instability in P_g between signals from Yucca Flat and Pahute is even more remarkable than that between MNV and KNB. There is a great increase in the complexity of P_g though the path differences for the two test sites are small. The most logical explanation is that strong scattering near the source is causing this difference. It is difficult to understand how such a strong effect would not interfere with spectral discrimination using P_g. The average P_n onset maintains its stable form and the ratio of P_n to P_g remains the same.

JAS In our earlier report, where we first described and characterized the onset of P_n, we worked with data from the DWWSSN stations Albuquerque and Jamestown. We showed that the split third swing was a very common observation at JAS and that the average waveform was very much like the one shown in Figure 4. The scattering of P_g is very strong for both test sites and the amplitude ratio of the two phases is 5 to 1.

ALQ The remainder of this section deals with stations at which interpretation of P_n waveforms is somewhat more problematical. At ALQ and ELK, the receiver structure seems to complicate the waveform slightly. At ALQ, the first swing of the waveform is consistently much more emergent than at other stations. Other than that, the waveshape is fairly consistent with those at other stations in the digital network. Figure 5 shows six observed signals from Yucca Flat events with varying depth. The feature associated with pP is indicated by arrows. Its timing with respect to the first energy is comparable to that observed at other stations, but the overall waveform is somewhat different. The depth dependence of the splitting feature is clear supporting the premise that it is related to the free surface interaction. The level of scattering of P_g is different between Yucca Flat and Pahute Mesa again being stronger for the former site. The amplitude ratio is comparable to that at other stations.

ELK The situation at Elko, Nevada is much like that at Albuquerque. The receiver function is somewhat complicated, but the physics of the wave propagation seems consistent with other sites. Figure 6 shows a representative set of waveforms with arrows indicating a feature that might be associated with pP. This type of variation of waveform due to receiver structure is not unexpected given that this is such high frequency data. At teleseismic (30° - 90°) ranges, short period WWSSN P waves have a relatively constant shape except at a small number of

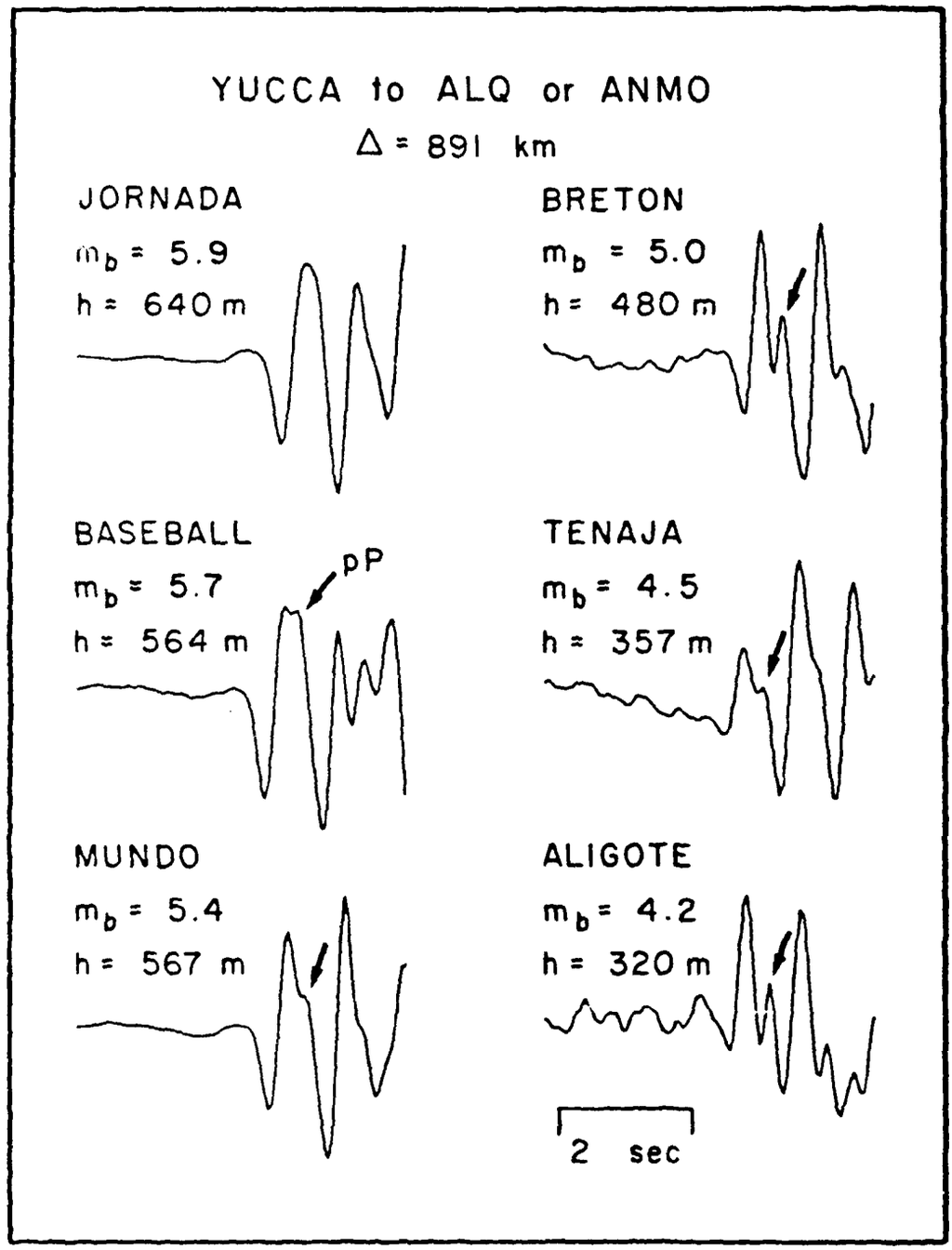

Figure 5. Observed P_n signals from Yucca Valley events at DWWSSN station ALQ. The split "c" swing is interpreted as the effect of pP_n. As events get larger, the increase in the duration of the source function washes out the pP effect.

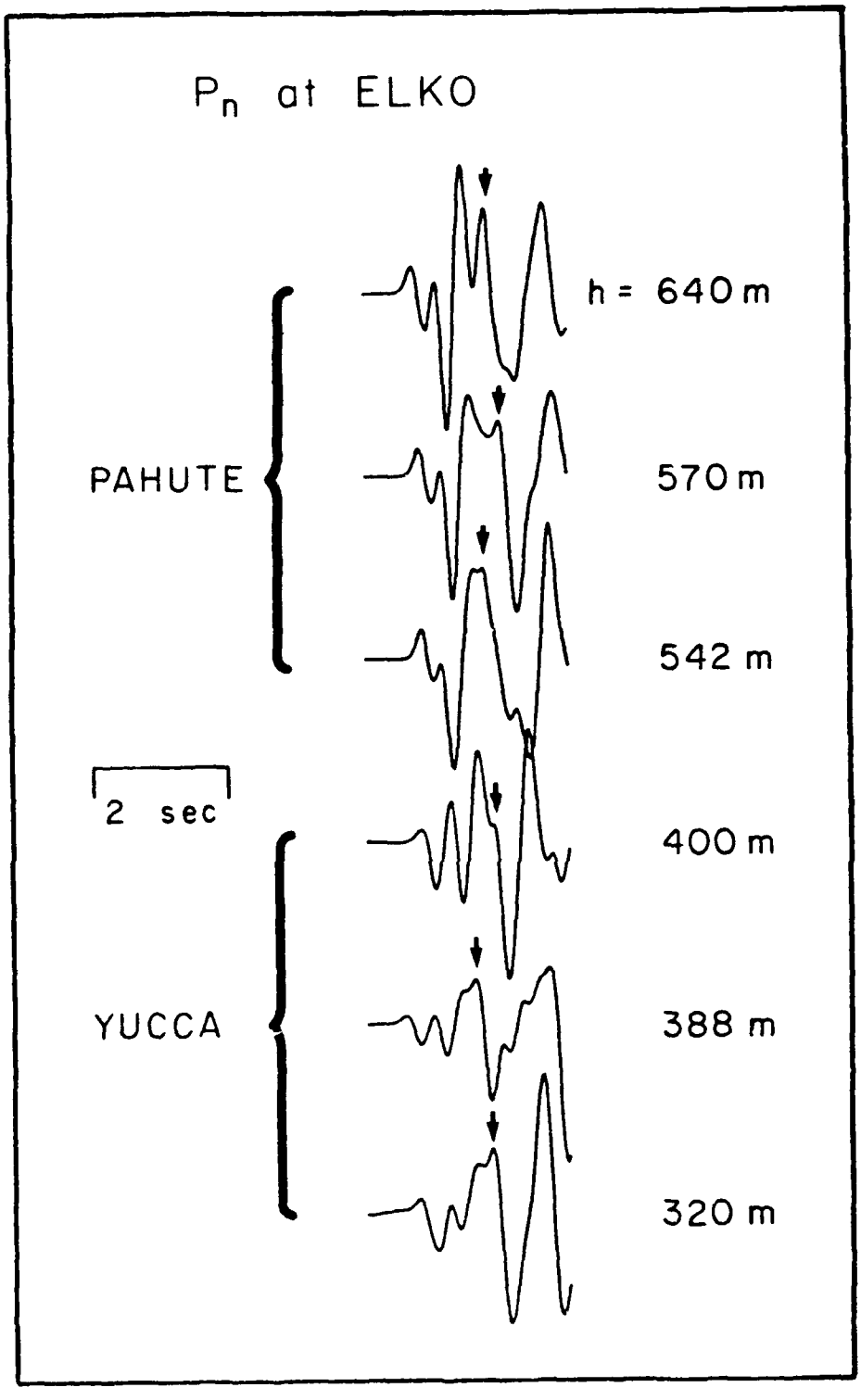

Figure 6. Observed P_n signals at ELK. The waveform shows additional complexity at the beginning. A feature which seems event depth dependent and might be associated with pP_n is indicated by arrows.

stations with complex receiver structures. Such variations can be removed by relative waveform analysis techniques (Burger et al., 1987). The other aspects of the regional P wave train at ELK remain constant.

PAS The reason that special note has been made in the preceding discussion of the ratio of P_n to P_g is that it varies markedly at stations to the south of NTS. The map in Figure 1 shows that these are at Landers, Pasadena and Pinyon Flat California. The latter two have only recently been upgraded to broad band digital stations with state-of-the-art Streckeisen instruments. Because they are relatively new, the available data from them are limited. At PAS, the waveform of P_n onset is not greatly different than at most stations in the digital network. Figure 7 shows the averaging of three waveforms to sum to a final result much like that in Figure 2 for MNV. However, there is a marked change in the relative amplitude of P_n at PAS as shown in Figure 8. On the top, are shown three regional P signals from Yucca events at JAS. It is illustrated in the appendix that these are signals typical of those from every station discussed to this point in terms of the P_n to P_g ratio. The bottom three traces are typical of those observed at PAS. The ratio has decreased from 5 to 1 to less than 2 to 1. The seismic sections in the appendix show clearly that PAS is different in this regard for both Pahute and Yucca Flat events. The reason is that the P_n is being amplified by a rapid velocity increase or discontinuity in the lid.

LAC The station at PAS is intermediate in range between LAC and PFO and is apparently located in the middle of the triplication. LAC is at the beginning. The events closest to LAC at a range of about 295 km have a normal P_n. P_n waveforms from several events are compared at stations MNV and LAC in Figure 9. The correspondence between waveforms is very strong indicating a simple and deterministic type of wave propagation. The scaling of frequency content with event size is very consistent between the two stations. At slightly greater

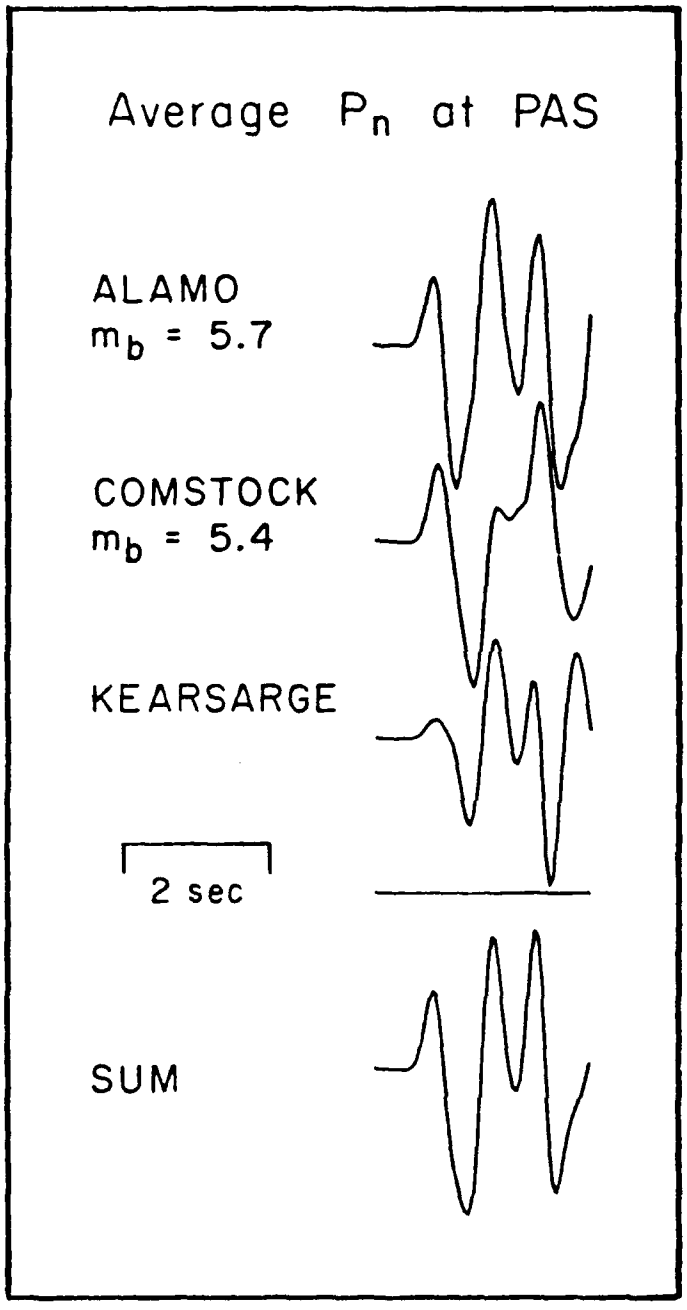

Figure 7. The average P_n waveform at PAS. The "c" swing is consistently split even though the P_n is being amplified due to a triplication.

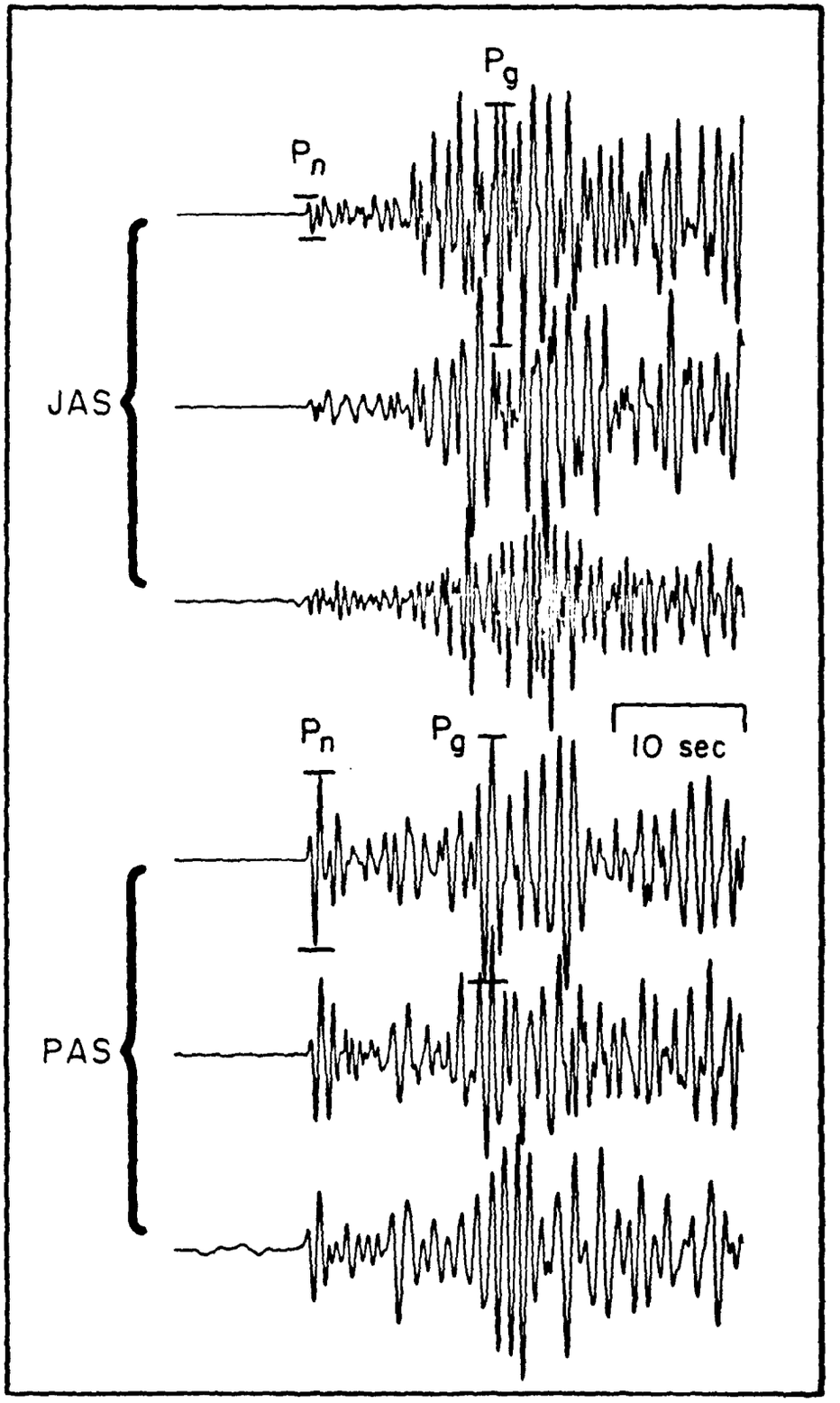

Figure 8. Amplification of P_n with respect to P_g at PAS. At JAS and all other stations not to the south of NTS, the ratio of the phases is about 5 to 1. At PAS and other southern stations it is less than 2 to 1.

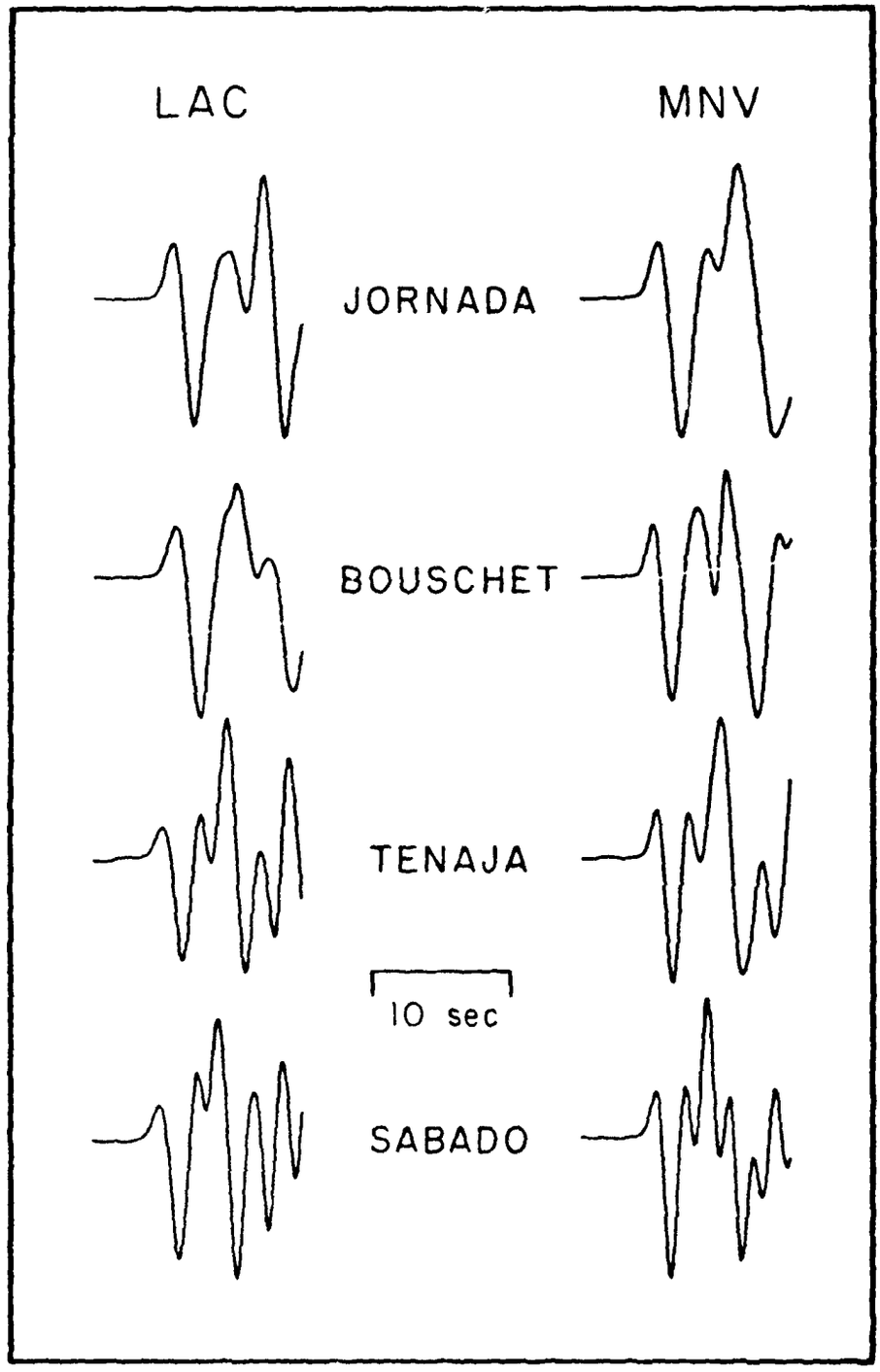

Figure 9. A comparison of P_n waveforms for common events at MNV and LAC. At these ranges the triplication has not begun to have an effect and the waveshapes are very similar.

ranges, the triplication clearly emerges, however, as shown in Figure 10. By about 315 km, a clear precursor has emerged ahead of a strong second arrival. The section in the appendix shows that P_n grows systematically with respect to P_g though not quite to the levels it reaches at PAS farther into the triplication. PFO As shown in the final sections in the appendix, the data available from Pinyon flat is very limited. The waveform of the P_n is relatively complicated, and the P_n to P_g ratio decreases with range. We interpret this as the end of the triplication. PFO may also have a complex receiver function, but resolving turning point from near receiver structural effects is beyond the scope of this investigation.

To quantify the P_n amplification effect, we have measured the P_n to P_g amplitude ratio on a set of the available records from the California stations. The P_n amplitude is defined as the RMS value within 5 s after the first arrival. The P_g amplitude is defined as the RMS value within 20 s after the arrival time of PmP as predicted by the Helmberger and Engen (1980) crustal model. This model appears from experience to be a good predictor of P_g onset. Since it has been made clear that the behavior of P_g varies between the Pahute Mesa and Yucca Flat test sites, it would be best to deal with data from only one site. More data are available from the Yucca Flat site, so at LAC, and PAS we have used data from only that site. Very little data are available from either site at PFO. Therefore, we used data from both test sites at this station. The resulting amplitude ratios are plotted as a function of distance in Figure 11. Certain features of the behavior are very clear, such as the relative amplification of P_n at PAS and PFO. The upward trend at LAC and downward trend at PFO are more questionable but are suggested by dashed lines in the figure.

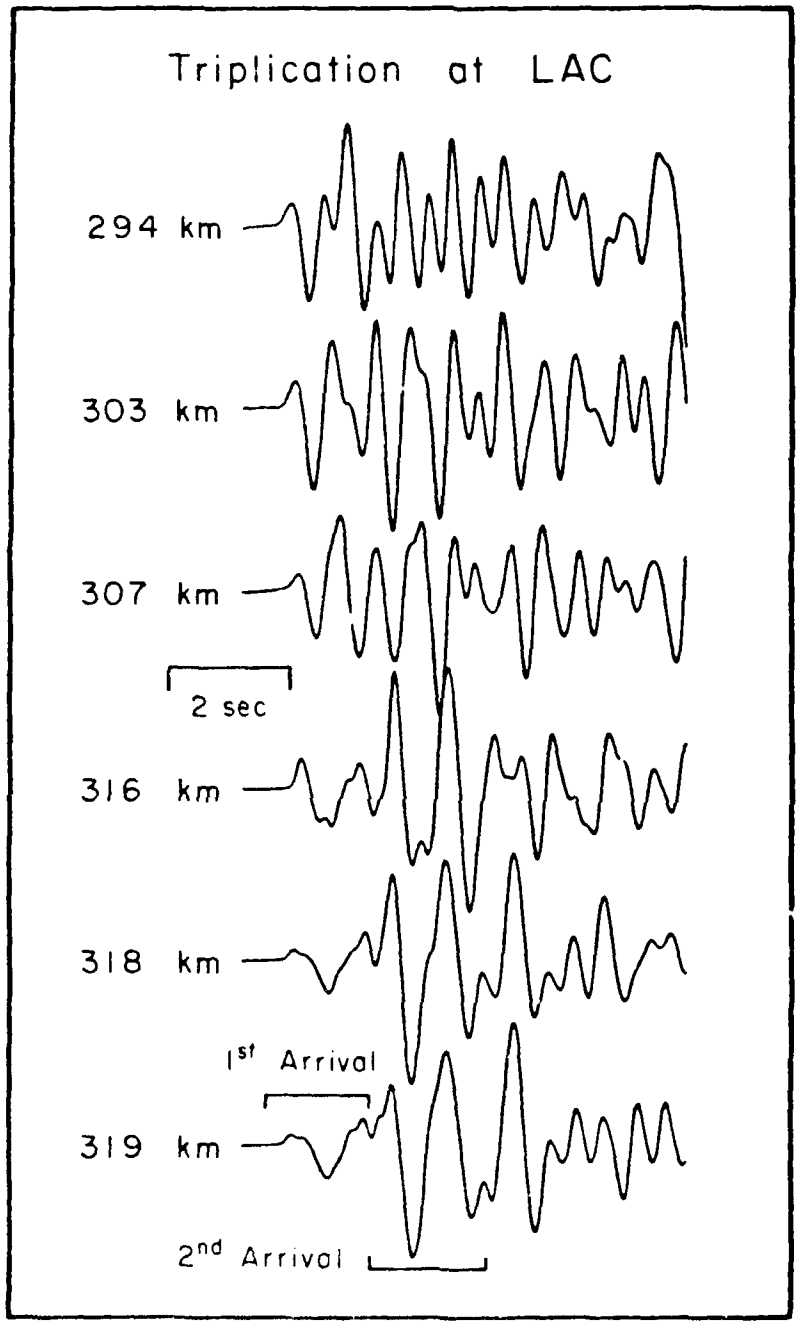

Figure 10. Development of the triplication with range at LAC. At the close ranges, the first energy is the largest and the P_n waveform is similar to that at most stations. At greater ranges, a large second arrival develops and moves toward the front of the record.

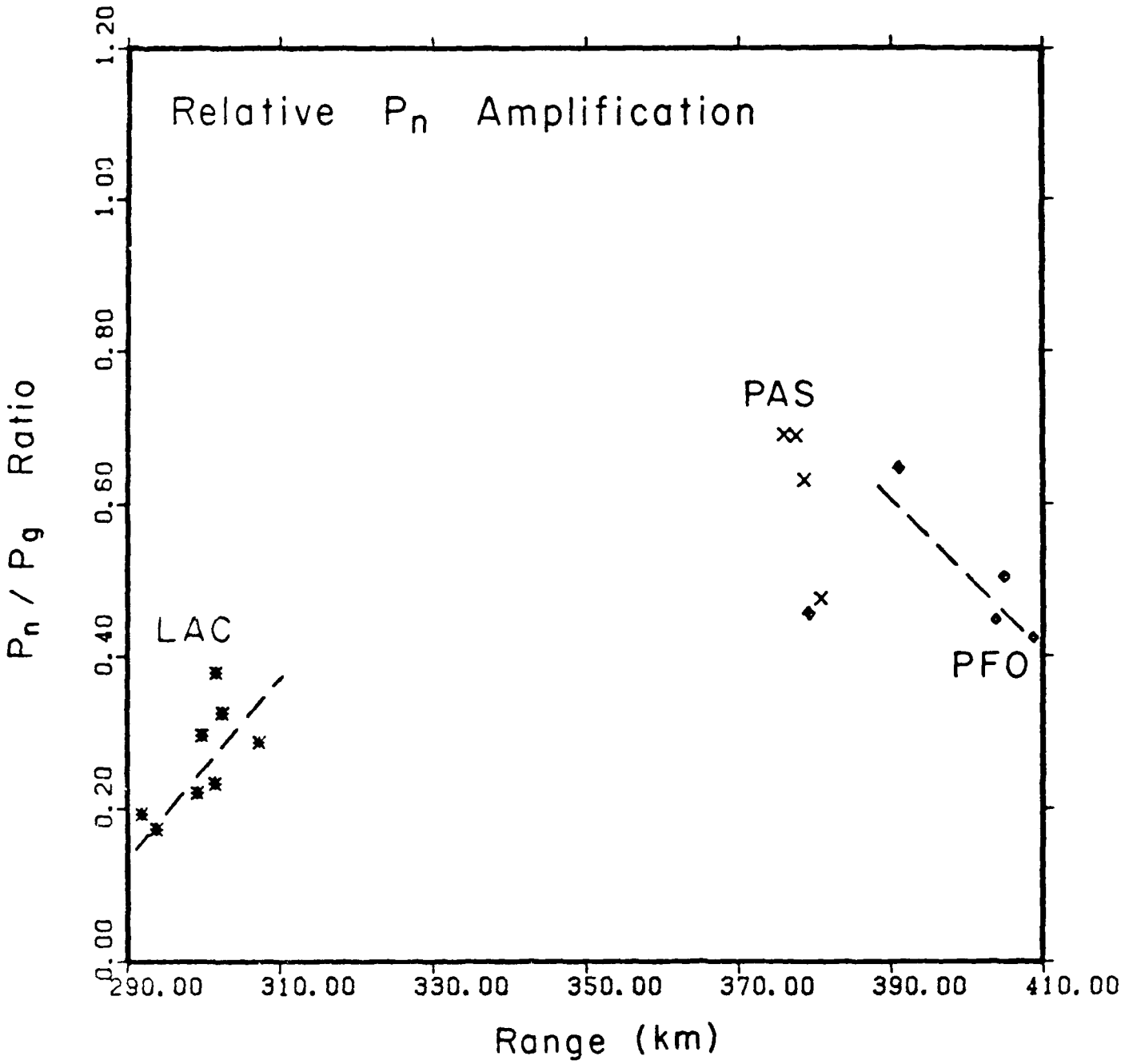

Figure 11. The ratio of the RMS amplitude/sec. of P_n to P_g with range. It is very clear that the ratio increases between LAC and PAS. Other trends which might be significant are indicated by dashed lines.

Results of the P_n Averaging Despite the preceding discussion of some of the complexities of P_n propagation in the western U. S., we believe that the importance of the phase is its stability and simplicity in most areas. Triplications due to structure in the lid are not a universal of the earth feature or they would have been noticed long before. The existence of one in this region is probably related to the intense tectonics of southern California. Such phenomena are less likely to occur in stable continent. We expect that there will always be some stations with complex receiver structures such as ELK, but if the discrimination procedure is based on observations from an array of stations this difficulty can be overcome.

The tests at Pahute Mesa are on average larger than those from Yucca Flat. The structure there also appears to be simpler and the scattering less intense. The pP effect seems in general to appear more consistently and more clearly for Pahute events. Figure 12 shows the average P_n for 5 stations in the digital network. The splitting of the "c" swing is indicated by arrows. The only stations in the digital network for which we do not show a result are ELK, LAC and PFO. The former has a complex receiver structure, and the latter two are affected by the triplication. Figure 13 shows similar averaging results for 7 stations. All of the digital stations except ELK and PFO are represented. We have obtained the result for LAC by averaging signals at ranges prior to the beginning of the triplication. We also show results from two analog stations, BFS and GSC. As we discussed in our previous report, we hand digitized the data from these stations and then averaged in the same way. Given the stability of the waveforms in the two figures, one would have to conclude that we are seeing a manifestation of a very fundamental property of explosion sources. We will show in the following that this property involves reflection of energy from these shallow sources from the free surface.

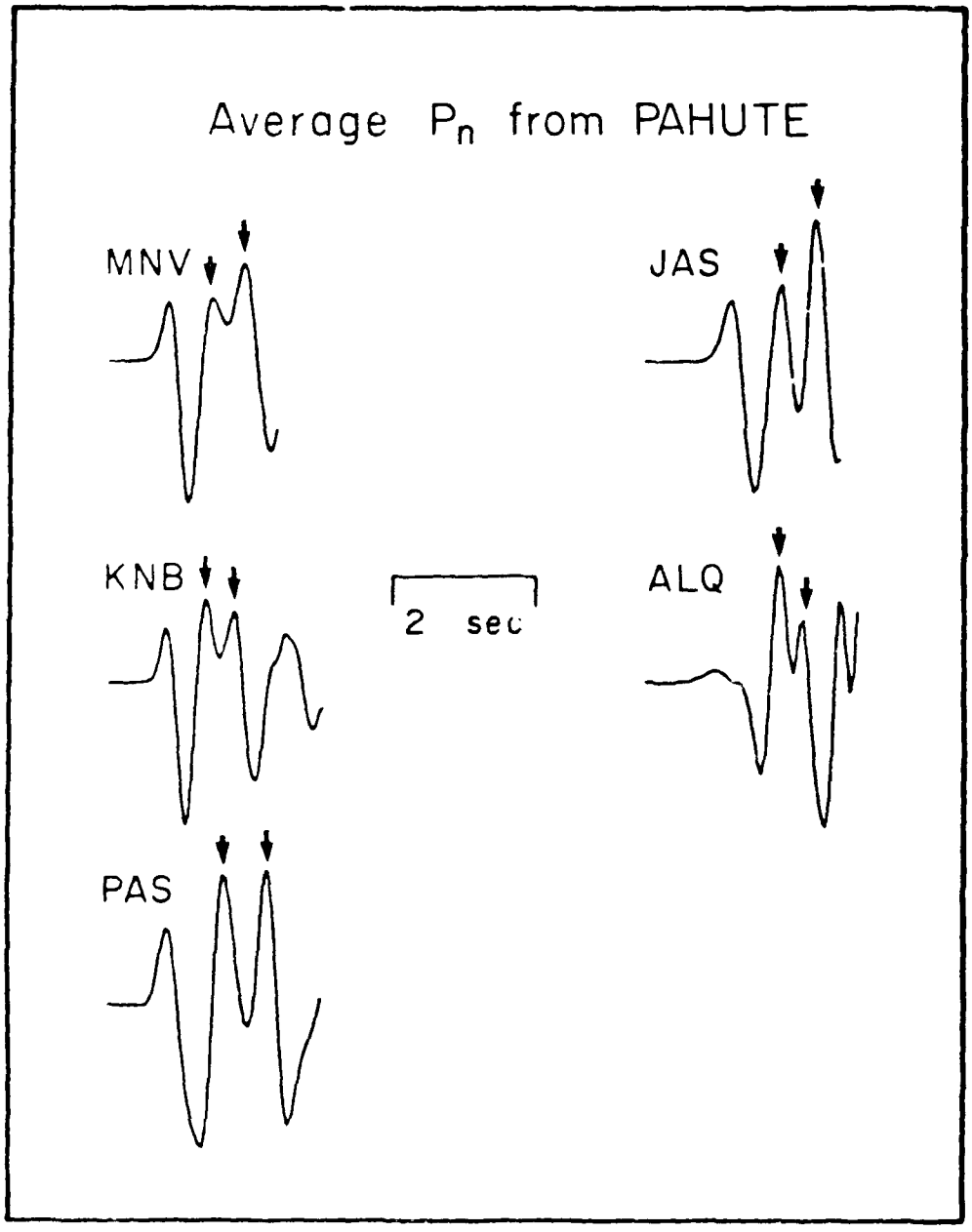

Figure 12. The average P_n waveform for Pahute events observed at stations in the western U.S. digital net. The split third swing is indicated by arrows.

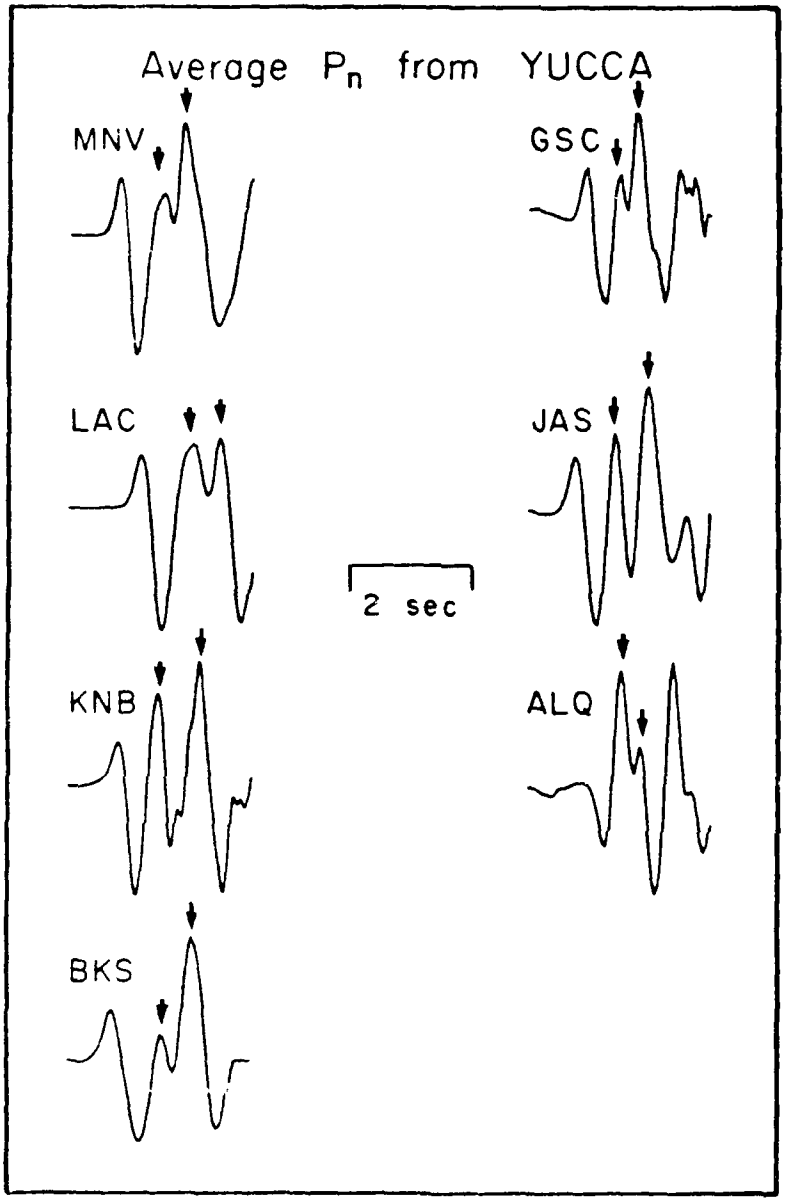

Figure 13. The average P_n waveform for Yucca events observed at stations in the western U.S. digital net. The split third swing is indicated by arrows.

MODELING OF THE WAVEFORMS

In the preceding discussion, we have dealt with signals with a uniform WWSSN short period response. In the modeling studies to be presented next, we will work with two of the LLNL stations where the pP effect is very clear. We will take advantage of the very broad band response of the LLNL instruments and deconvolve the instrument response out. We will work with actual ground velocity traces and show that the effect of pP is simple and straightforward to understand.

The theoretical instrument response function for the LLNL stations was developed and presented by Vergino et al. (1986). They also discussed the procedure for deconvolving the response out to generate true ground velocity. (In this instance, deconvolution simply implies inverse convolution whereas it has been used in other cases to imply more complex procedures.) With the instrument effect removed, we can represent an observed velocity trace V(t) in the standard synthetic body wave decomposition as

$$V(t) = S(t) * G(t) * Q(t)$$

where S is the source, G is the elastic response of the earth and Q is a correction for anelasticity. The * represents convolution. For the purposes of this discussion it is convenient to further decompose the elastic response G(t) into

$$G(t) = G_s(t) * G_t(t) * G_r(t)$$

These three subresponses represent the effect of structure near the source, turning point and receiver respectively. Such a decomposition is justified for short times near the first arrival. $G_s(t)$ contains the effects of the free surface and near source crust. $G_t(t)$ contains the effects of structure near the turning point if any or the effect of the ray turning process itself. At complex receiver sites such as ELK, $G_r(t)$ would have a major effect. In the following, we shall model data from the simple sites at MNV and KNB. We will neglect the effects of this last operator. Each of the operators in this general decomposition

have been studied and characterized extensively in the past but apparently not using the regional P_n waveform. The data set assembled in this study presents a unique opportunity to do so.

The most recent work on the nuclear explosion source function S(t) by Murphy (1988) indicates that it can be well approximated by the Mueller Murphy representation for Pahute wet tuff for all test sites providing the events are well coupled and below the water table. There is a need for further testing, however, of both whether the functional form of the Mueller Murphy source is appropriate and whether the yield scaling is supported by the data. The common assumption regarding $G_t(t)$ is that it can be represented at short times by a step function. This corresponds to the standard wave front expansion from ray theory for a head wave (Aki and Richards, 1980). In the following, we will explore the possibility that it might be better represented by a delta function. In terms of the same wave front expansion theory, this would correspond to the P_n onset actually being energy turning in the lid. That is to say that rather than velocity being constant beneath the Moho it increases gradually with depth. Forward calculations show that even a weak gradient will cause the turning point response to evolve into a delta function rather than a step function very quickly. The question of how strong the correction for attenuation should be has been debated for many years for both teleseismic and regional P waves (Burger et al., 1987). It has generally been observed that both P_n and S_n follow a relatively high Q path.

In the following, we will present accurately computed synthetics for realistic crustal structures and compare them to observations. However, we begin with a simple schematic calculation to illustrate the features of most importance in the data and the synthetics. Figure 14 shows this calculation. The top trace is the Mueller Murphy source function for velocity assuming a turning ray. It has been convolved with a Futterman operator with a t^* level set at 0.1 s. If

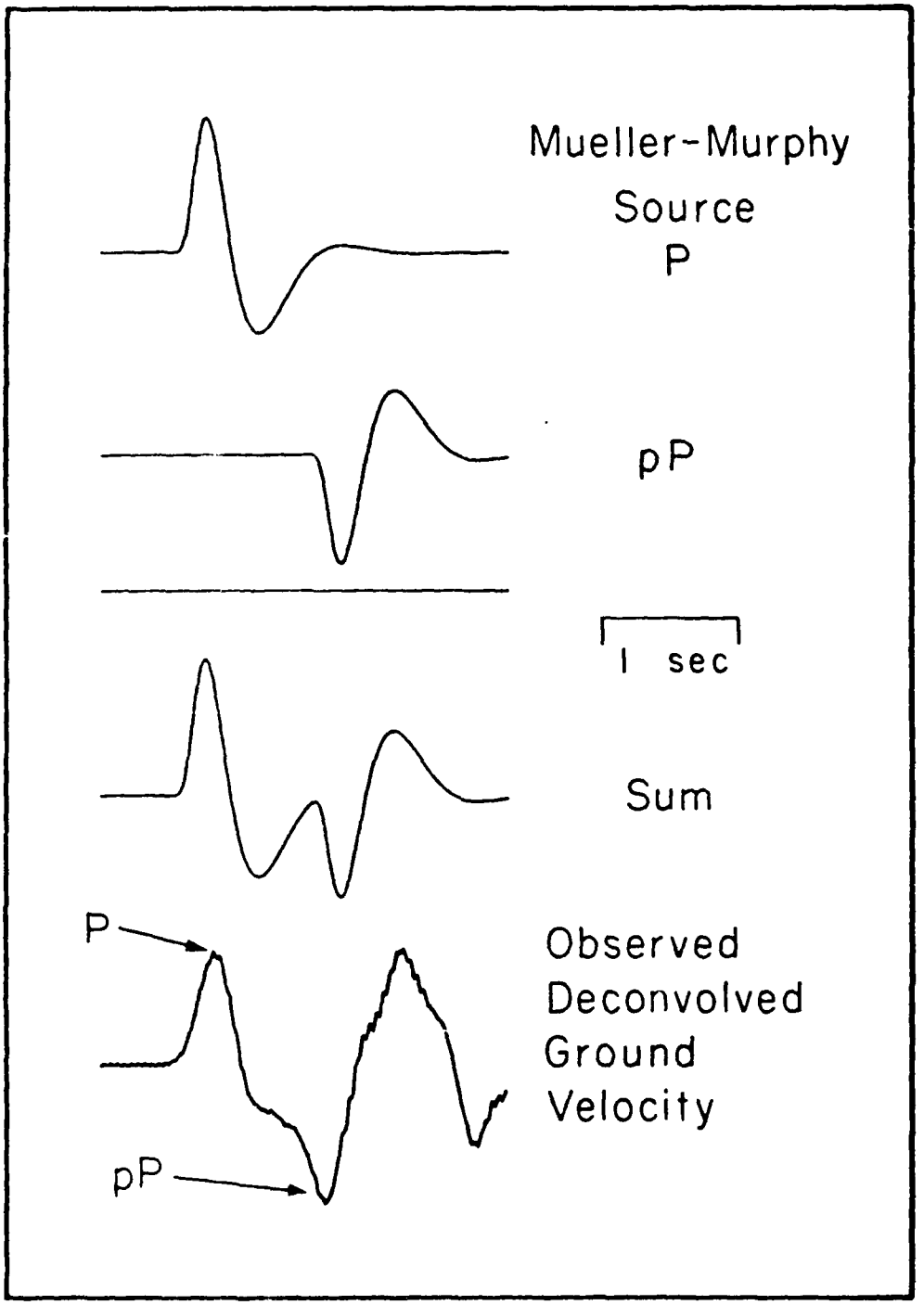

Figure 14. A simplified synthetic calculation indicating the expected effect of elastic pP_n on the ground velocity trace. It lengthens the downswing and adds a second upswing. An observed trace from MNV is shown at the bottom. The features associated with P and pP in the data are indicated by arrows.

a head wave model for P_n is assumed this pulse would simply be integrated. The second trace represents elastic pP_n. It is reversed in sign, delayed and reduced in amplitude. In this simplified calculation, the resulting synthetic in the third row is just the sum of the first two traces. The direct P_n results in first an upswing and then a downswing. The pP_n results in the opposite. The effect of pP_n is to cause a shoulder in the P_n and to extend its duration. The observed P_n ground velocity from Yucca flat event JORNADA is shown at the bottom. The features associated with the direct and pP arrivals are indicated by arrows.

The calculation shown in Figure 14 is highly approximate in that the delay time and relative amplitude of pP_n have been set arbitrarily. These values along with the effects of crustal structure should be computed from an accurate model of the NTS crust. In the following, we compute the response $G_s(t)$ using standard layer matrices and an assumption of constant slowness. The crust model we use is based on modeling studies of near field data and has been shown to be accurate for timing purposes (Hartzell et al., 1983). We use the appropriately scaled Mueller Murphy source for S(t) and again a Futterman operator for Q(t).

Figures 15 and 16 compare data to synthetics for four Pahute Mesa events as observed at MNV. From these calculations, we hope to address a number of questions. These include, is the turning ray or head wave model for $G_t(t)$ more appropriate, does the Mueller Murphy source scale correctly and what is an appropriate value of t^* for P_n? We also would like to know whether the commonly used approximation of pP as an elastic reflection of P is accurate.

The results for the turning ray approximation of $G_t(t)$ are shown in Figure 15 and for the head wave in 16. We began by simply assuming that the Mueller Murphy source gives the correct source pulse shape S(t). Because the Mueller Murphy source assumes an f^{-2} spectral decay rate, the predicted velocity pulse

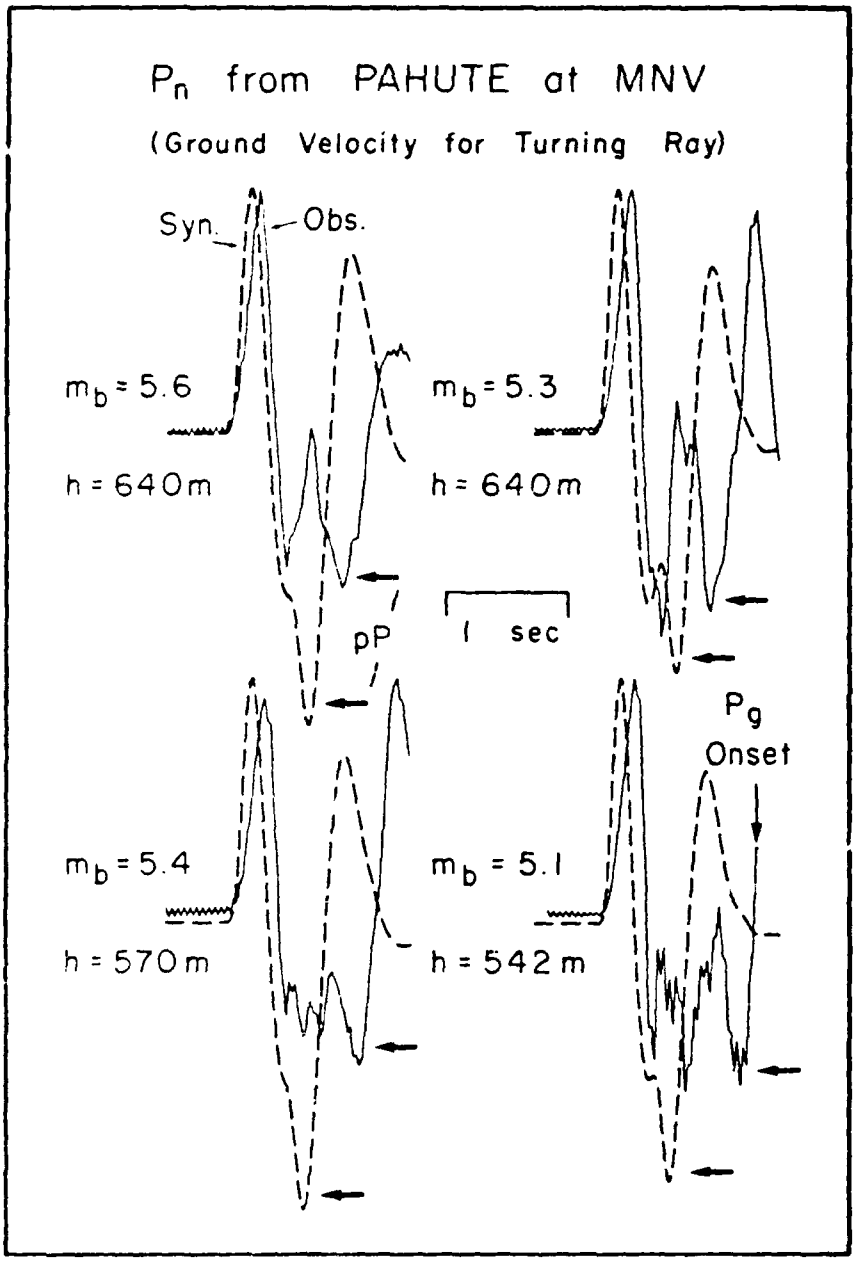

Figure 15. Observed versus synthetic P_n waveforms at MNV for Pahute events. The turning ray model for propagation is assumed. The Mueller Murphy source scaling relations and a t^* value of 0.1 s are also assumed. As indicated by arrows, the observed pP arrival is late but approximately the same in size as the elastic prediction.

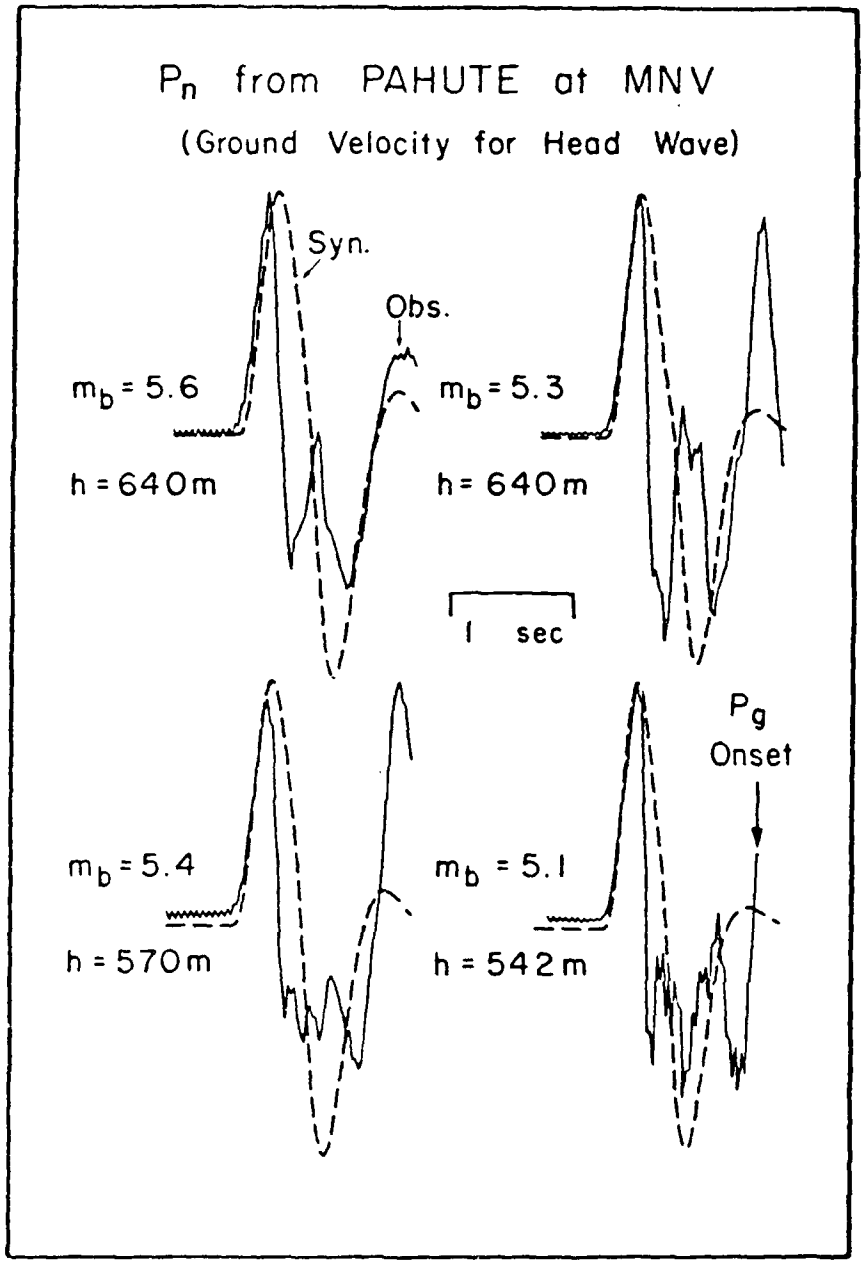

Figure 16. Observed versus synthetic waveforms at MNV for Pahute events. All assumptions are the same as for Figure 15 except for a head wave model for propagation.

is discontinuous. We increased the level of attenuation (t^*) until the discontinuous pulse was smoothed into approximately the observed pulse. There are two features of the observed pulses to be considered. The first is the zero to peak or rise time. The second is the duration of the first swing. The t^* value for the synthetics in Figures 15 and 16 was ultimately set at 0.2 s. The comparisons in Figure 15 show that for the turning ray model, this value gives approximately the right duration for the first swing but that the theoretical rise time remains too high. The latter discrepancy could mean that the f^{-2} spectral decay assumption is incorrect or that a frequency dependent Q correction is required. The Mueller Murphy source scaling predicts a larger difference in the durations of the largest and smallest events than is observed. This is a small data sample, but it would appear that the possibility that the scaling effect is too strong in the Mueller Murphy formalism will need further exploration in the future. The computed pP arrivals and what we interpret as pP arrivals in the data are indicated by arrows. The observed pP is clearly and consistently later than the predicted. This phenomenon of anomalously delayed pP has been observed consistently in teleseismic data in many different investigations involving many different approaches (Murphy, 1988; Lay, 1985). The P_n waveforms confirm this anomaly. The only interpretation warranted is that what appears as pP_n or teleseismic pP is more complex than a simple elastic reflection. The observed amplitude and waveshape of pP in the figure is comparable to the predictions. Unfortunately, the traces had to be truncated after only two seconds because of the onset of P_g (see Figure 2).

The head wave synthetics in Figure 16 do not fit the observations nearly as well as the turning ray synthetics. Because of the additional integration, the synthetic pulses become much too long in period. The shoulder associated with pP_n onset washes out completely. The value of t^* was adjusted to match the

observed rise time of the pulses. As the figure indicates, it is impossible to simultaneously match the rise time and the duration of the first peak while using the head wave model for P_n.

Similar comparisons between data and synthetics for Yucca Flat events observed at MNV are shown in Figures 17 and 18. In this instance, a t^* value of 0.1 s appears most consistent with the data. The match between observations and synthetics in the top two traces of Figure 17 is extraordinary. There can be little doubt that a feature associated with the free surface interaction is being modeled. It is again clear, however, that this feature arrives too late to be elastic pP_n. It also appears that in some cases pP_n has a larger amplitude than direct P_n. This could only be caused by some nonlinear effect in the source region. Under the circumstances, it is probably best to refer to the pulse as effective pP_n and not to attempt to model it too closely using assumptions of perfect elasticity. The pP_n from the magnitude 5.4 event at the lower left shows additional structure. This is another indication that a complex process is occurring.

The Mueller Murphy source scaling again fails to predict variations in frequency content associated with source size. There is a large shift in frequency content between the top events with magnitude 5.7 and 5.9 which the scaling law does not predict. There is a modest increase in frequency content as source size decreases from m_b 5.7 to 5.4 to 4.5, but the scaling laws over predict the effect. The head wave model synthetics in Figure 18 are uniformly too low in frequency content. This reinforces the credibility of the turning ray representation of the P_n arrival.

Similar comparisons of data from Pahute and Yucca Valley at station KNB are shown in Figures 19, 20, 21 and 22 respectively for the same events modeled at MNV. We will not discuss these comparisons in extended detail, but we believe

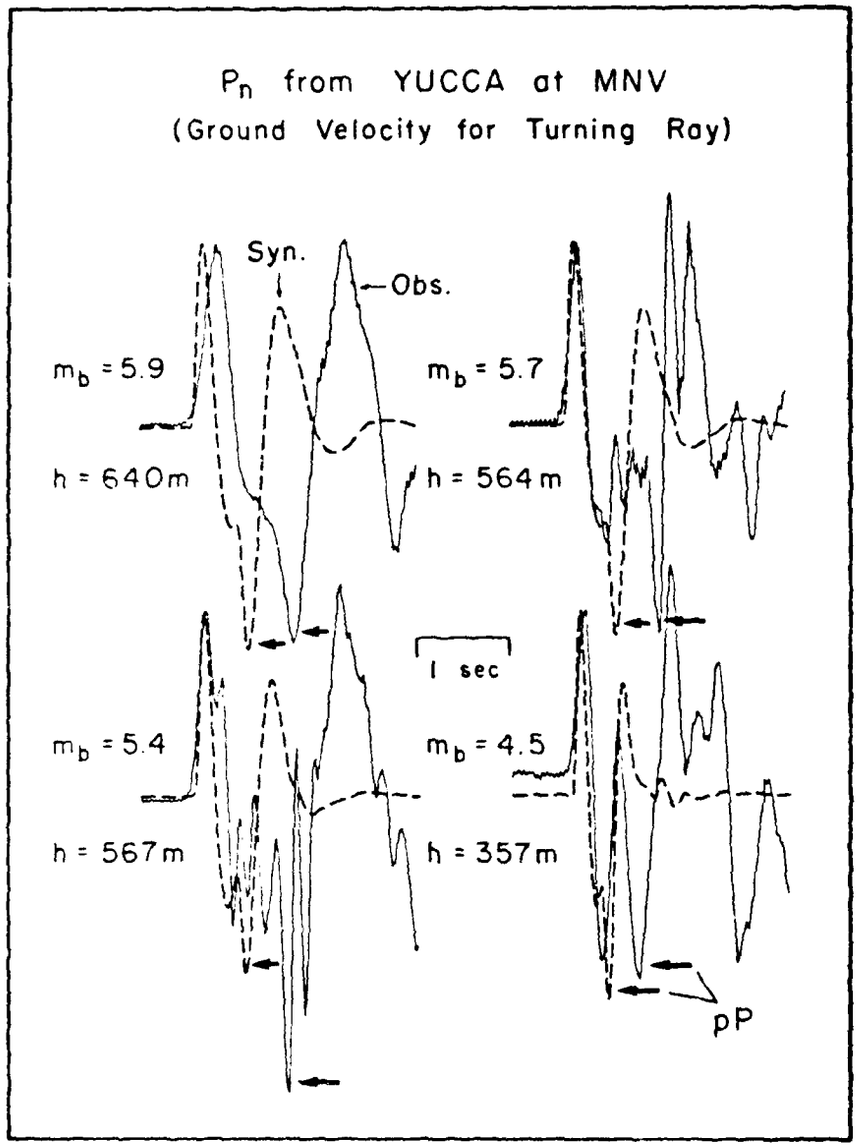

Figure 17. Observed versus synthetic waveforms at MNV for Yucca events. All assumptions are the same as for Figure 15 except for an increase in t^* from 0.1 to 0.2 s.

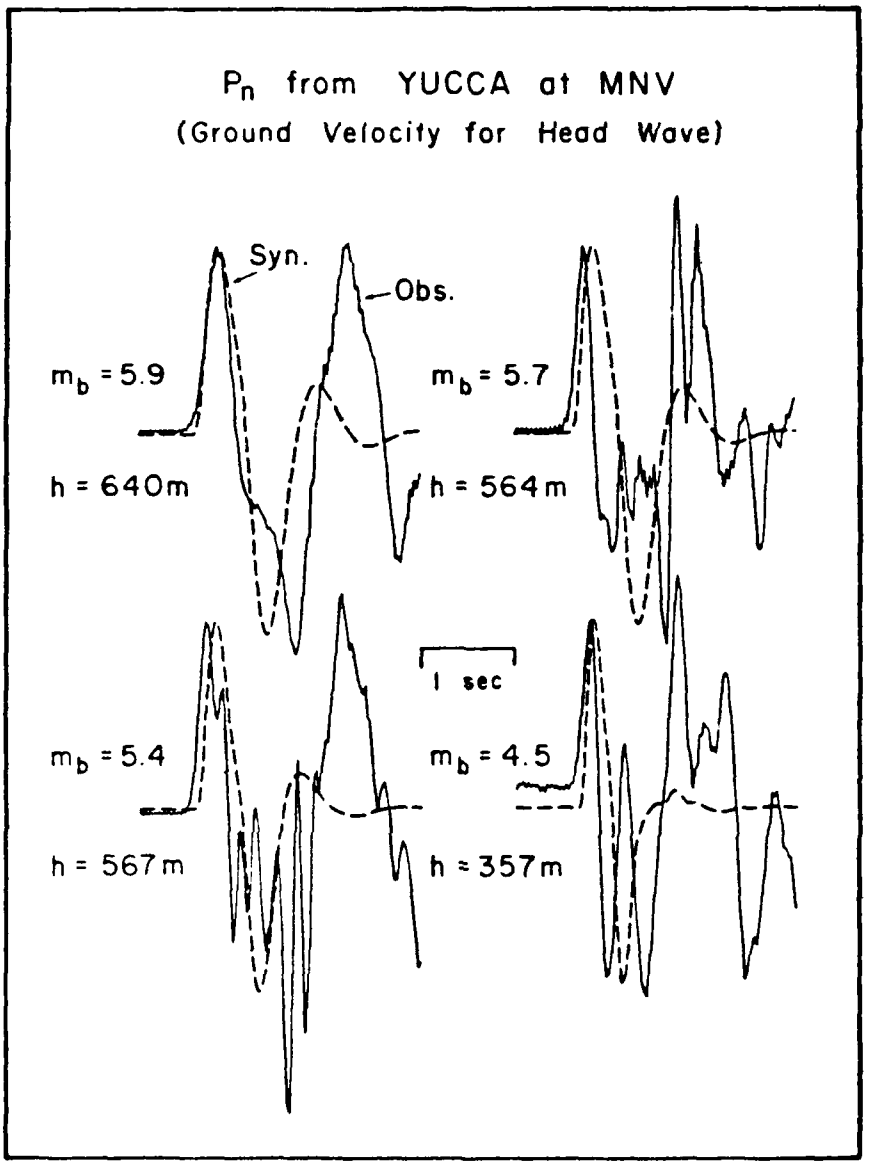

Figure 18. Observed versus synthetic waveforms at MNV for Yucca events. All assumptions are the same as for Figure 15 except for a head wave model for propagation and an increase in t^* from 0.1 to 0.2 s.

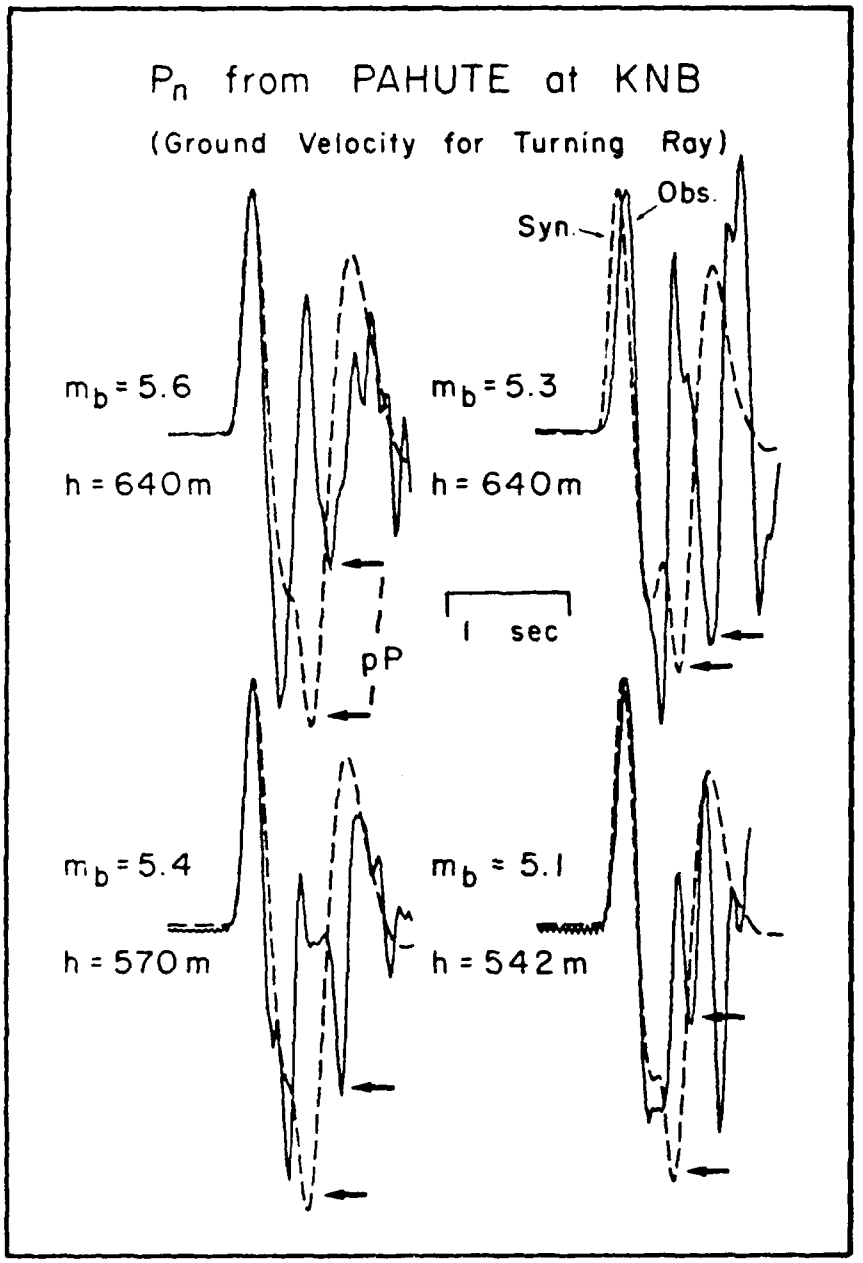

Figure 19. Observed versus synthetic waveforms at KNB for Pahute events. All assumptions are the same as in Figure 15.

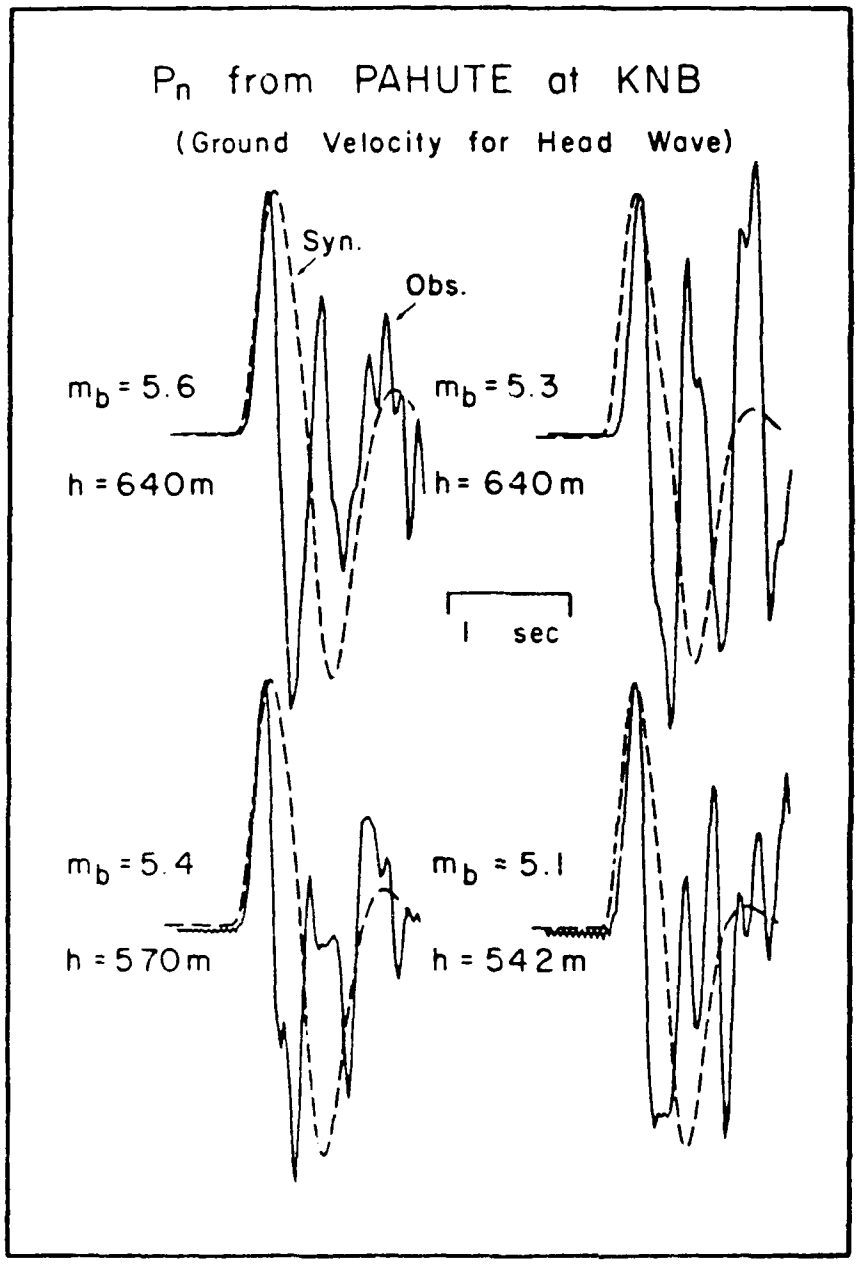

Figure 20. Observed versus synthetic waveforms at KNB for Pahute events. All assumptions are the same as in Figure 16.

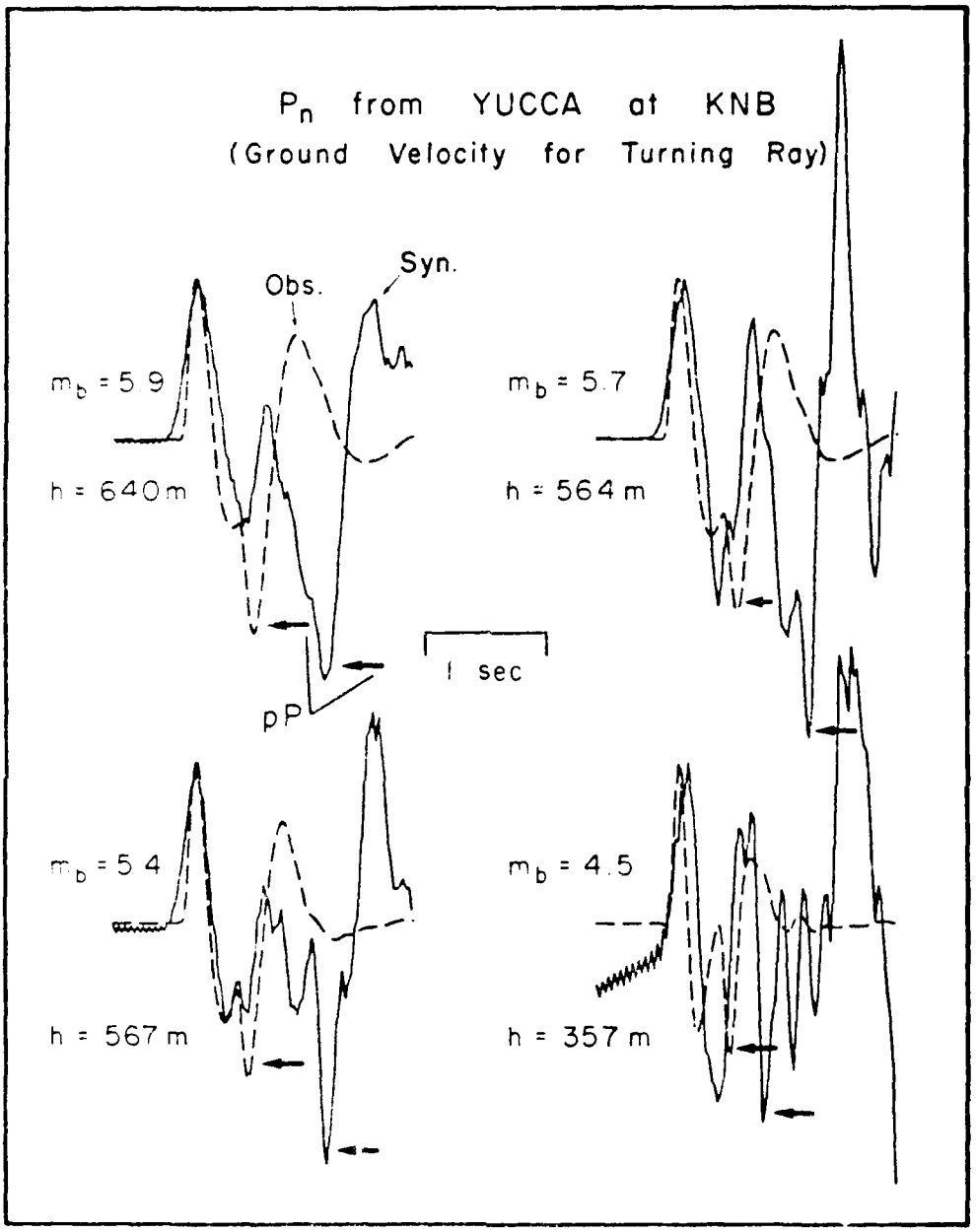

Figure 21. Observed versus synthetic waveforms at KNB for Yucca events. All assumptions are the same as in Figure 17.

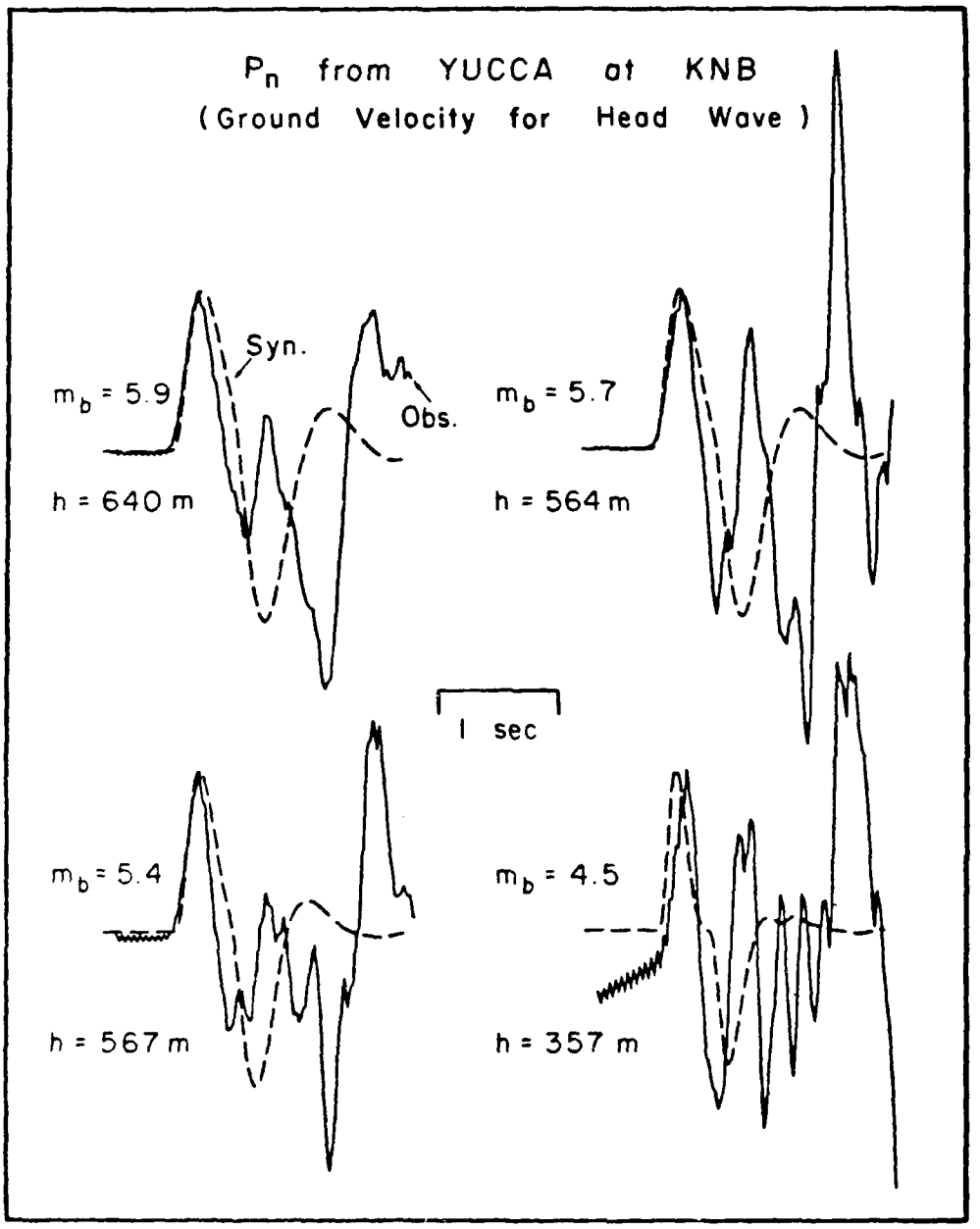

Figure 22. Observed versus synthetic waveforms at KNB for Yucca events. All assumptions are the same as in Figure 18.

they illustrate the following points. Effective pP_n is always present as indicated by the arrows. It is always significantly later than the elastic predictions. For Pahute events, the amplitude of effective pP is approximately the same as for the elastic predictions. For Yucca Valley events it is consistently larger. The physics of effective pP generation appears to be test site dependent. The value of t^* appears to be about 0.1 or 0.2 s for P_n. This is almost an order of magnitude decrease from the value for teleseismic P. The head wave model for $G_c(t)$ consistently produces synthetics which are too long period to fit the observations. The Mueller Murphy scaling laws do not successfully predict the observed frequency shifts for Yucca Valley events.

DISCRIMINATION WITH THE P_n WAVEFORM

Figures 12 and 13 demonstrate that the P_n waveform is on average very stable and that it exhibits a distinctive feature a few seconds after onset. The above modeling studies provide a convincing case that this feature is associated with effective pP_n. Since earthquakes uniformly occur much deeper than explosions, it is reasonable to expect that few earthquakes will exhibit a highly similar feature at such short times into the waveform. In a previous report (Burdick et al., 1988), we demonstrated in a quantitative way that this was the case. We collected P_n waveforms from the earthquakes mapped in Figure 1 at stations ALQ and JAS. We windowed out 3 second onset waveforms from both the earthquake and explosion signals and measured their correlation with an analytic norm. This norm has been described in detail by Burdick (1986). It attains a maximum value of 1.0 if and only if two waveforms are identical. Figure 23 shows the result of measuring the correlation of Pahute explosion versus earthquake waveforms with the average explosion waveform from ALQ. Pahute signals seem to be more consistent in their pP_n character than Yucca signals. The discrimination of explosion from earthquake signals is very good at all stations just as in Figure 23. Unfortunately, the majority of events detonated at Pahute Mesa are large. Standard techniques could be used to discriminate them from earthquakes. Smaller magnitude explosions are usually detonated at Yucca Flat, and because of the greater instability of pP_n discrimination is somewhat more problematical there.

Figure 24 shows the results for Yucca Flat events at ALQ. The discrimination performance of the waveform norm definitely deteriorates between magnitude 4.0 and 4.5. However, a careful review of this deterioration shows that it is caused at least in part by a signal to noise ratio problem. ALQ is the most distant station in the digital net, so this might not be so much of a problem at other stations. Also, it generally seems that P_n signal to noise ratio is much better

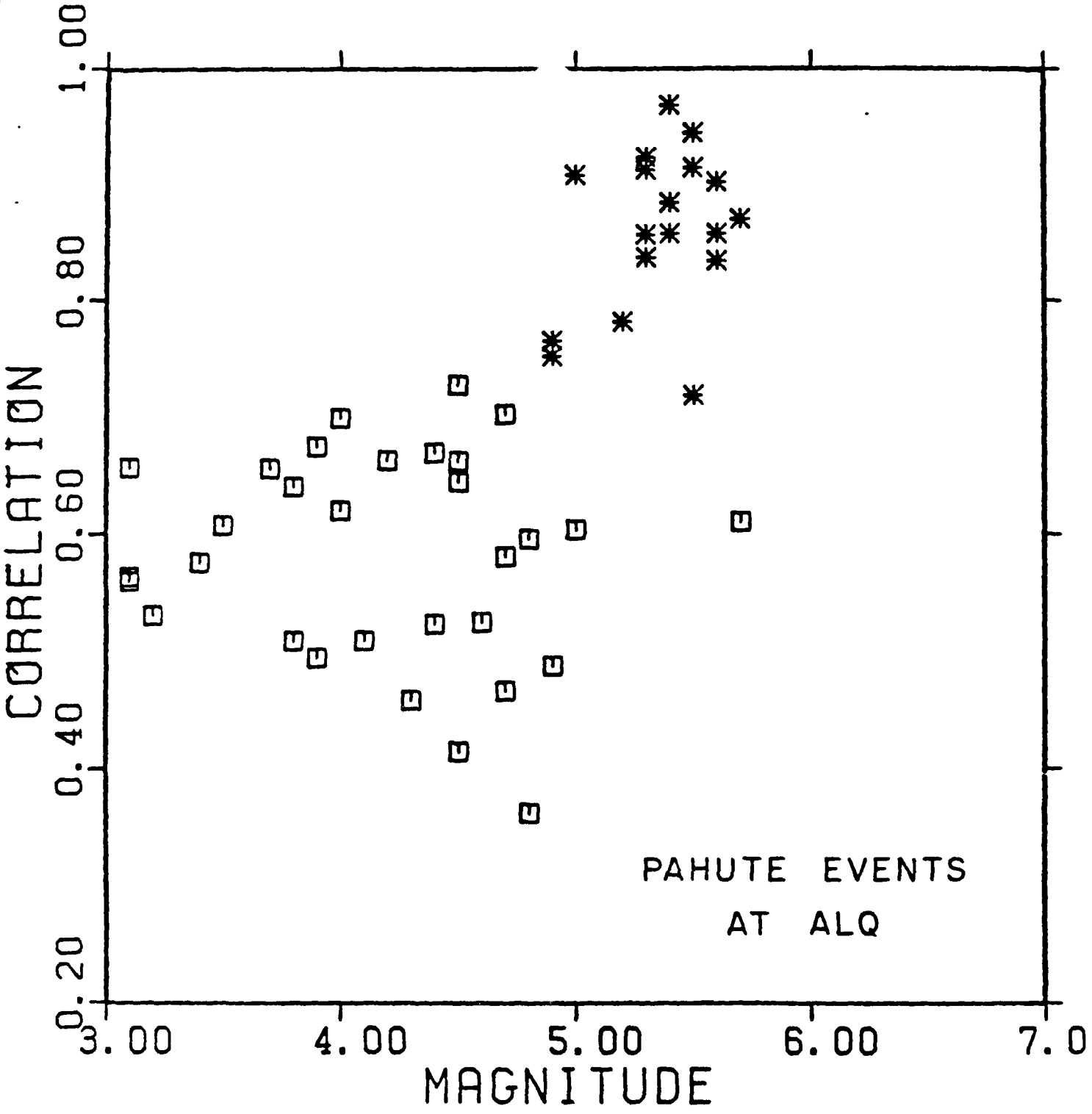

Figure 23. Discrimination of Pahute explosions from earthquakes using correlation with the average P_n waveform at ALQ. The explosions are stars and the earthquakes squares.

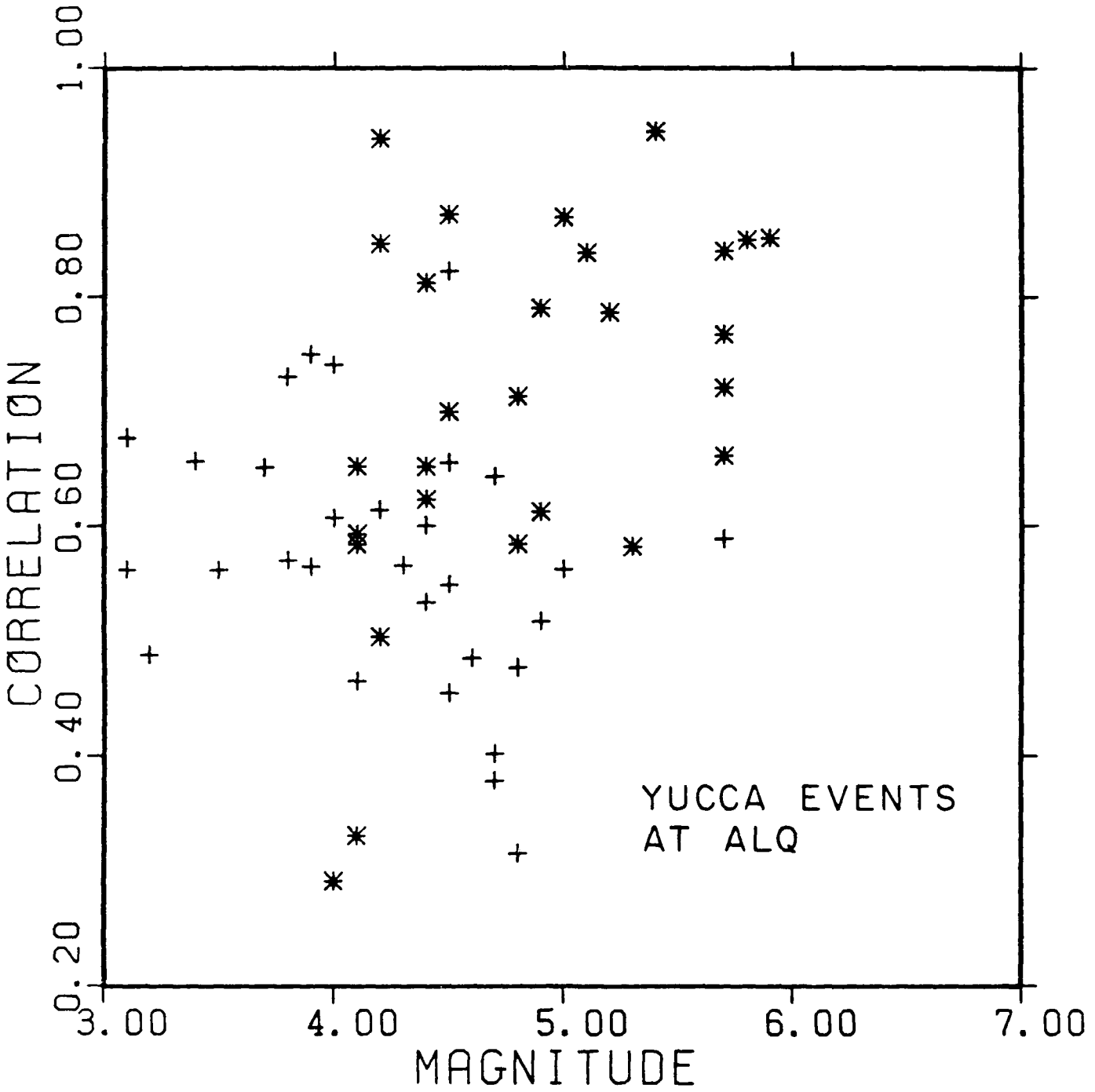

Figure 24. Discrimination of Yucca explosions from earthquakes using correlation with the average P_n waveform at ALQ. The explosions are stars and the earthquakes crosses.

in stable continental regions than in the highly tectonized western U.S. Figure 25 shows the discrimination results for Yucca Flat events at JAS. The separation of explosions from earthquakes between 4.0 and 4.5 is somewhat improved.

A further consideration in developing a discriminant based on P_n waveform is that some dependence of the waveform on event size should be expected. In the examples of the waveform discriminant shown so far, we have simply tested for the correlation of waveforms with the average waveforms shown in Figures 12 and 13. Generally those averages were formed from signals of larger events since they tend to exhibit the splitting of the third swing more clearly. To estimate the importance of event size on the waveform discriminant, we averaged explosion P_n waveforms at JAS from six explosions with magnitude between 4.0 and 5.0. The correlation of that waveform with the JAS discrimination data base is shown in Figure 26. The correlation of the large explosions with the average waveform clearly with respect to the levels in Figure 25. The discrimination efficiency at small event size clearly improves. It appears that as the waveform discriminant is developed further, an event size correction should be incorporated into it.

The discrimination tests shown so far demonstrate only that explosion P_n waveforms are consistent and stable at regional stations and systematically different than earthquakes. The conditions of the tests are, however, highly idealized. In a realistic situation, signals will be recorded on a regional array from continuously varying azimuths. The discrimination procedure would have to assimilate all of the waveforms from the array and test whether the signals had a feature resembling explosion pP_n on average. The consistency of the P_n waveforms in Figures 12 and 13 indicates that such a procedure should be effective at some level. A simple test as to whether explosion pP_n signals from one station can be used to discriminate between events at another station has been made by correlating the average MNV signal with the JAS data set. The

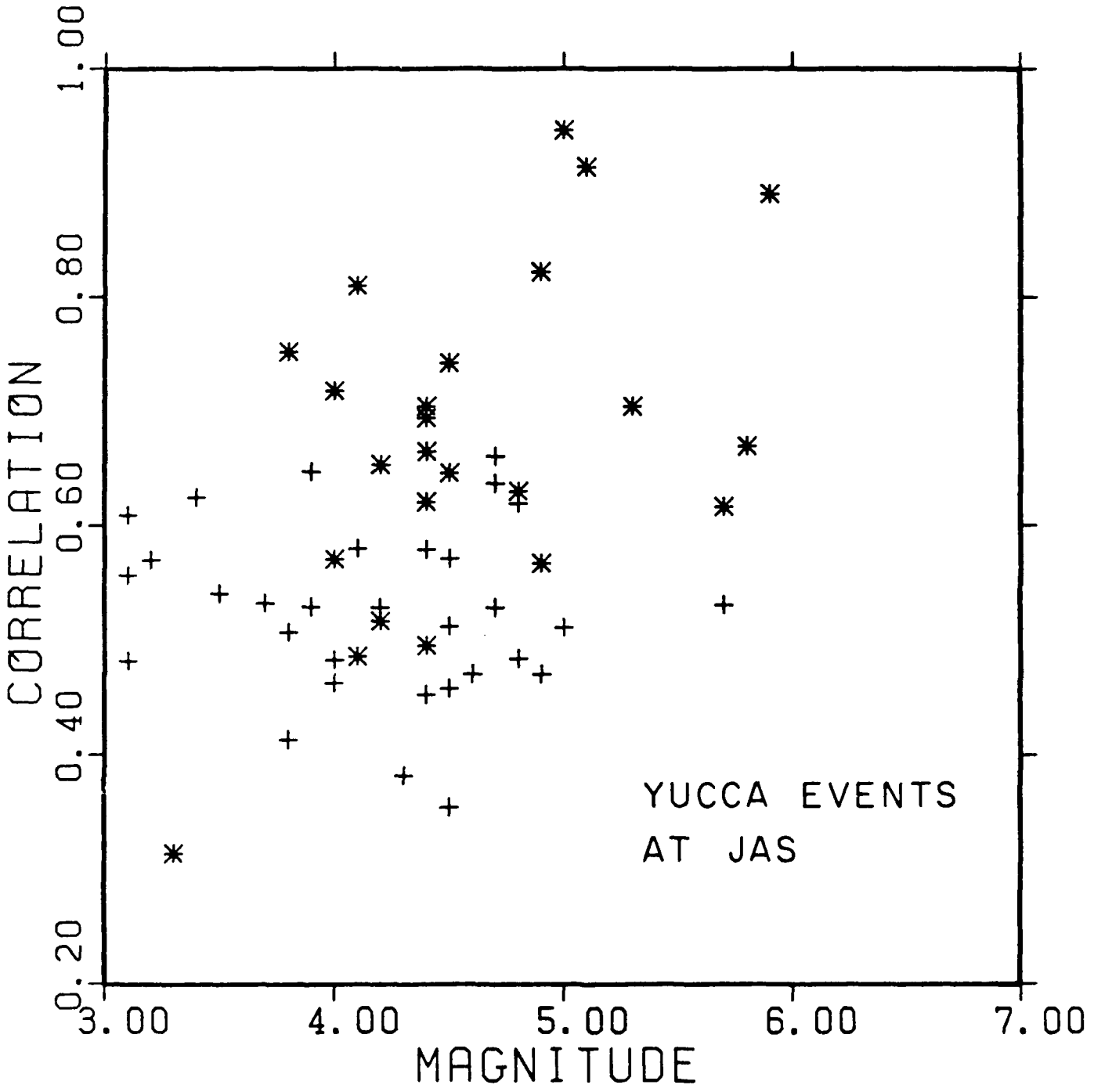

Figure 25. Discrimination of Yucca explosions from earthquakes using correlation with the average P_n waveform at JAS. The explosions are stars and the earthquakes are crosses.

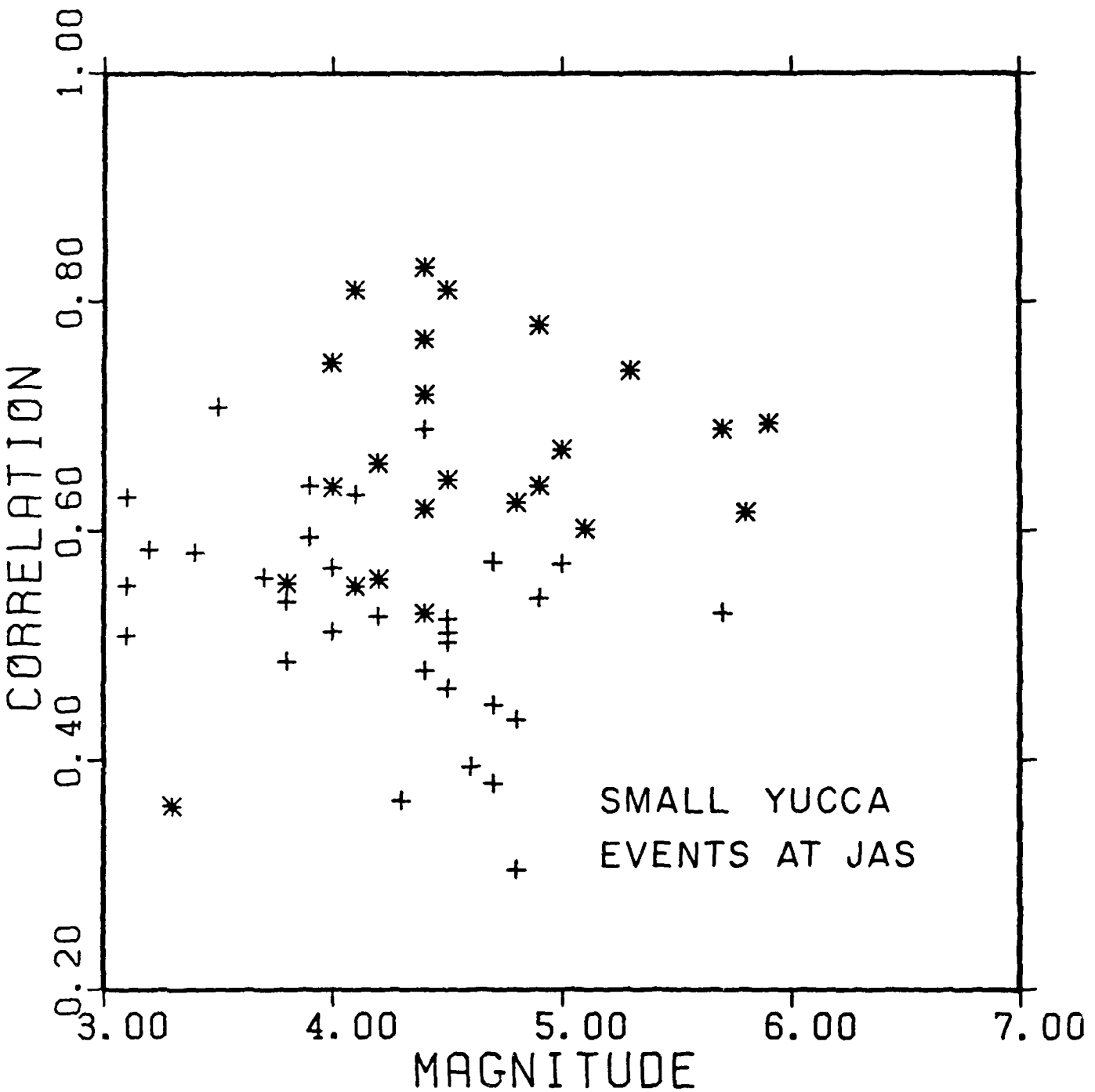

Figure 26. Discrimination of Yucca explosions from earthquakes using correlation with an average P_n waveform explicitly formed by averaging signals from smaller events. In comparison to Figure 25, discrimination is better for small events and poorer for large events. This is presumably an effect of source scaling.

results are shown in Figure 27. The discrimination efficiency is comparable to the level achieved with the JAS waveform proving the feasibility of the waveform discriminant.

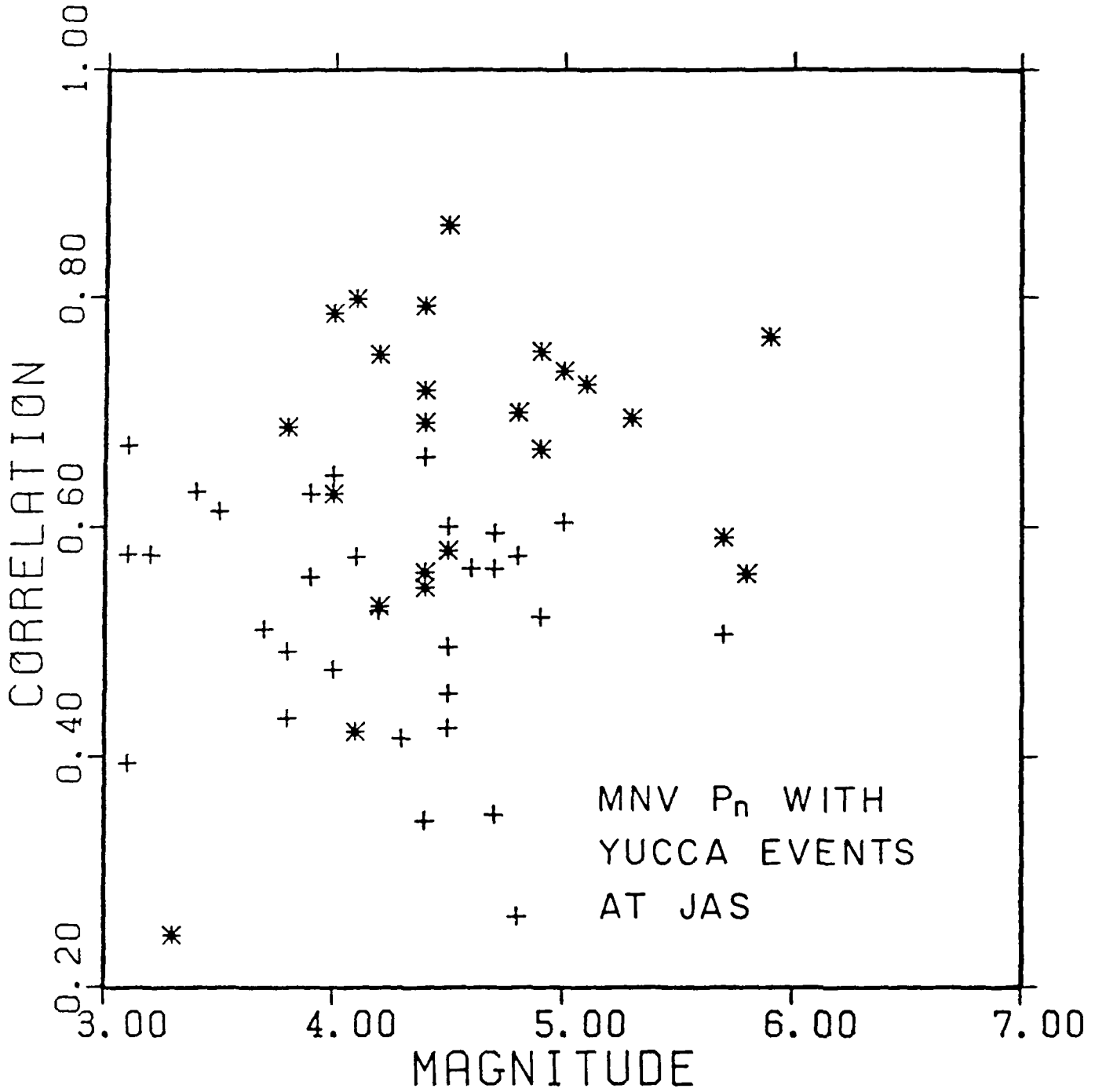

Figure 27. Discrimination of Yucca explosions from earthquakes using the average P_n waveform from MNV and the data base from JAS. Explosions are stars and earthquakes are crosses. The separation of the populations is comparable to that in Figure 26 illustrating the transportability of the discriminant.

DISCUSSION

There are balancing concerns involved in the development of an effective regional discrimination procedure. On the one hand, a high degree of reliability is desired, but on the other so is a dependable level of transportability. In the western U.S., the spectral discriminant of Taylor et al. (1988) seems to be more effective than the P_n waveform discriminant as it has been developed here. The difficulty with the former is that the physics behind it is not understood. Most lines of evidence involving, for instance, near field or teleseismic data indicate that there is no consistent spectral difference between explosions and earthquakes. Thus there is no way to be sure that the processes which cause this difference in the western U.S. will occur consistently in other regions. The P_n waveform discriminant is based on detecting the effects of the interaction of seismic energy with the free surface. Albeit these interactions are apparently nonlinear and not completely understood, they will occur for any nuclear test. The P_n waveform discriminant can be reliably transported.

Further development of the waveform discriminant should involve the collection and analysis of performance statistics in the western U.S. How often does a signal from a western U.S. earthquake correlate highly with a P_n signal from an explosion? It could be expected that similar performance statistics would hold in a region where actual verification was taking place. Some adjustment to the discrimination procedure and to the performance statistics could be based on studies of P_n waveforms from earthquakes in more normal tectonic regimes than the western U.S. The actual implementation of the discriminant on a computer could follow one of several approaches. One would be an empirical one in which observed waveforms from a regional net are continuously correlated with the average explosion P_n waveforms from the western U.S. digital net. Another approach could be based on synthetic modeling. The models could be adjusted to fit the

western U.S. P_n data base and then used to predict waveforms for other regions. Corrections for source scaling and for variations in attenuation would be straightforward to implement in this approach. A third method could be based on recognition of patterns in the waveform. For example, the method could be based on logical identification of the "c" swing and a logical test for whether splitting was occurring.

CONCLUSIONS

The waveform of the onset of P_n has been found to be extraordinarily stable in character in the western U.S. The waveform for nuclear explosions can be easily synthesized using standard models and methods. The specific modeling studies described here demonstrate that at high frequency P_n is more probably a turning ray from a gradient in the lid than a true head wave along the Moho discontinuity. The value of t^* for P_n appears to be in the range of 0.1 to 0.2 seconds. This means that the explosion source process can be observed in much closer detail than it can from teleseismic data where t^* values are closer to 1.0. The scaling laws for the Mueller Murphy source do not explain the observed scaling of P_n waveforms adequately. The effective pP_n can be observed clearly in the waveform. It differs in character between Pahute Mesa and Yucca Flat events. In all cases, it appears that simple elastic reflection from the free surface is a poor model for effective pP_n. The arrival time is always late with respect to direct P_n, and for Yucca Flat the pP_n is larger than direct P_n. The waveform of pP_n varies substantially in many cases from the direct arrival. It has been demonstrated here that the waveform of P_n can be used as the basis of a discrimination procedure.

REFERENCES

Aki, K. and P. G. Richards, Quantitative Seismology: Theory and Methods, W. H. Freeman and Company, San Francisco, 1980.

Burdick, L. J., "Estimation of the frequency dependence of Q from ScP and ScS phases", Geophys. J. R. A. S., 80, 35-55, 1985.

Burdick, L. J., C. K. Saikia and N. F. Smith, "Discrimination using P_n and Pg", AFGL-TR-88-0167, 1988. ADA202018

Burger, R W., T. X. Lay and L. J. Burdick, "Average Q and yield estimates from the Pahute Mesa test site", Bull. Seism. Soc. Am., 77, 1274-1294, 1987.

Everendon, J. F., C. B. Archambeau and E. Cranswick, "An evaluation of seismic decoupling and underground nuclear test monitoring using high frequency seismic data", Rev. Geophys., 24, 143-215, 1986.

Hartzell S. H., L. J. Burdick and T. X. Lay, "Effective source functions for Pahute Mesa nuclear tests", Woodward Clyde Consultants Report, WCCP-83-03, Woodward Clyde Consultants, Pasadena, CA, 1983.

Lay, T. X., "Estimating explosion yield by analytical waveform comparison", Geophys. J. R. A. S., 82, 1-30, 1985.

Murphy J. R., "Network averaged teleseismic P wave spectra for underground explosions part II: Source characteristics of Pahute Mesa explosions", Bull. Seism. Soc. Am., (submitted), 1988.

Murphy, J. R. and T. J. Bennett, "A discrimination analysis of short period regional seismic data recorded at Tonto Forest Observatory", Bull. Seism. Soc. Am., 72, 1351-1366, 1982

Savino, J. M., C. B. Archambeau and J. F. Masso, "VFM discrimination results from a 10 station network", VSC-TR-81-29, Systems Science and Software, La Jolla, California, 1980.

Taylor, S. R., N. W. Sherman and M. D. Denny, "Spectral discrimination between NTS explosions and western United States earthquakes at regional distances", Bull. Seism. Soc. Am. 78, 1563-1579, 1988.

Vergino E. S., M. D. Denny and S. R. Taylor, "Discrimination of NTS explosions and western United States earthquakes: data processing", Lawrence Livermore National Laboratory, UCID-20689, Livermore, California, 1986.

von Seggern, D. H., and D. W. Rivers, "Seismic discrimination of earthquakes and explosions with application to the southwestern United States", SDAC-TR-77-10, Seismic Data Analysis Center, Alexandria, Virginia, 1979.

APPENDIX 1.

SEISMIC SECTIONS OF NTS EVENTS FROM THE WESTERN U.S DIGITAL ARRAY

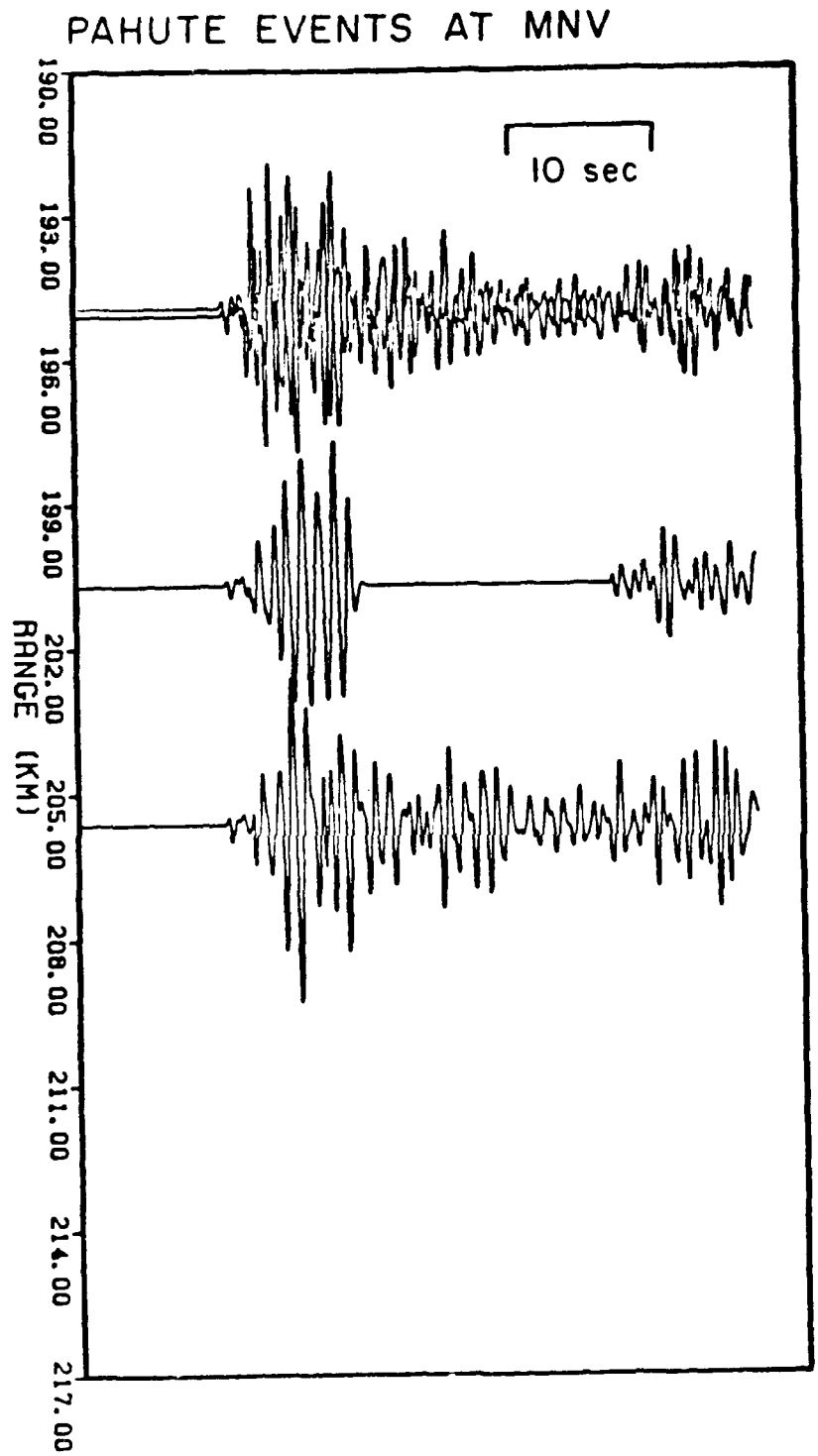

Figure A1. A seismic section of Pahute events observed at MNV.

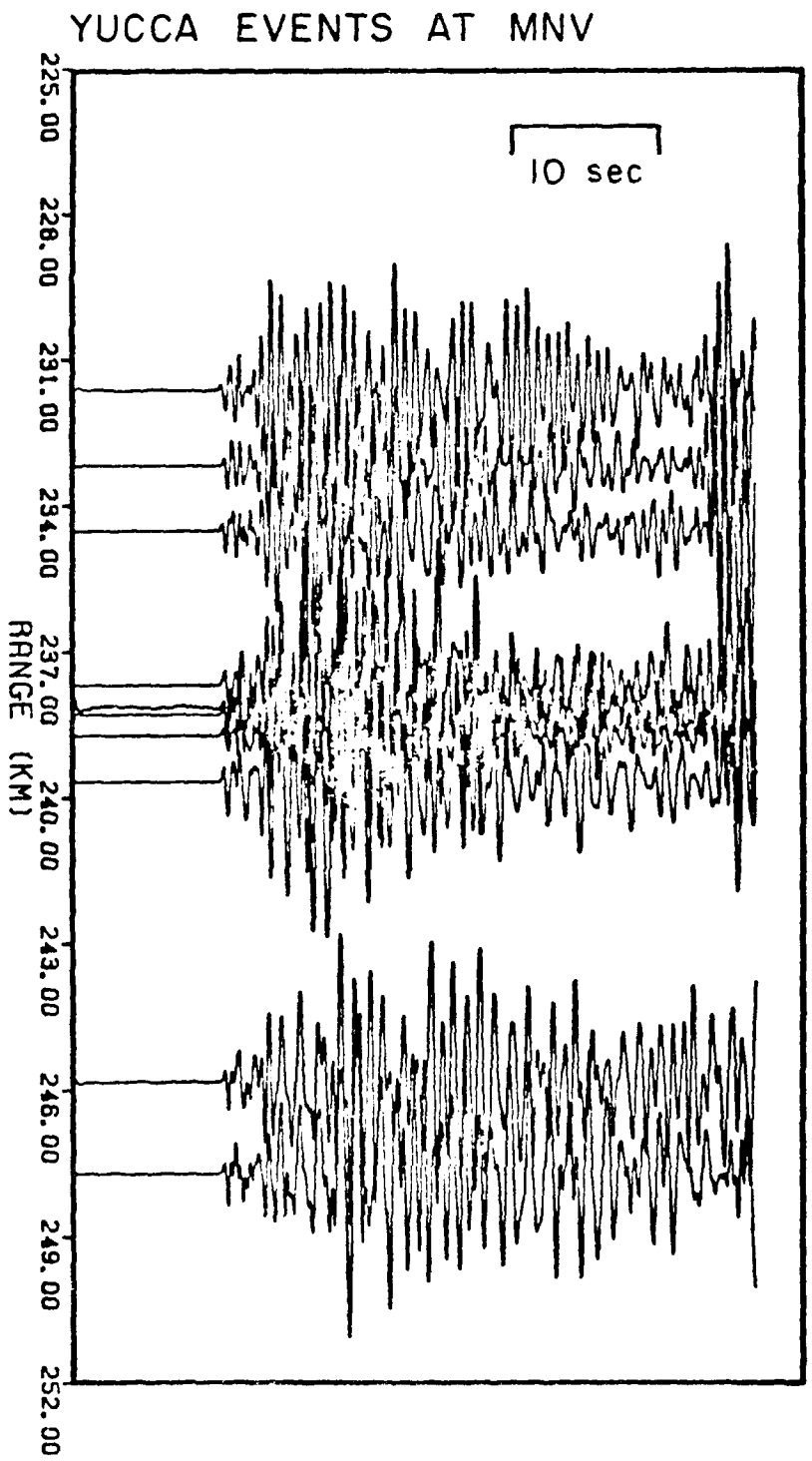

Figure A2. A seismic section of Yucca events observed at MNV.

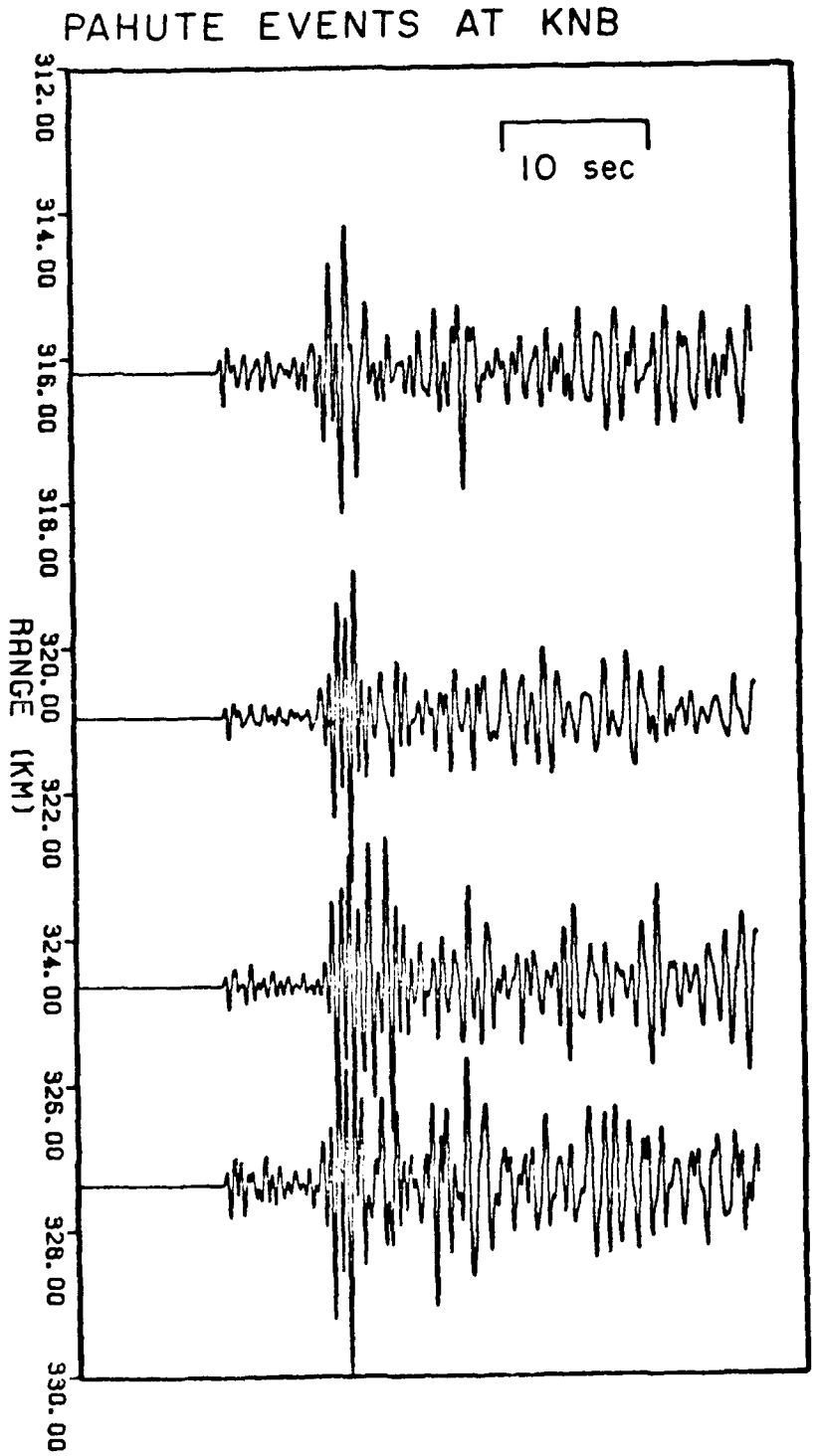

Figure A3. A seismic section of Pahute events observed at KNB.

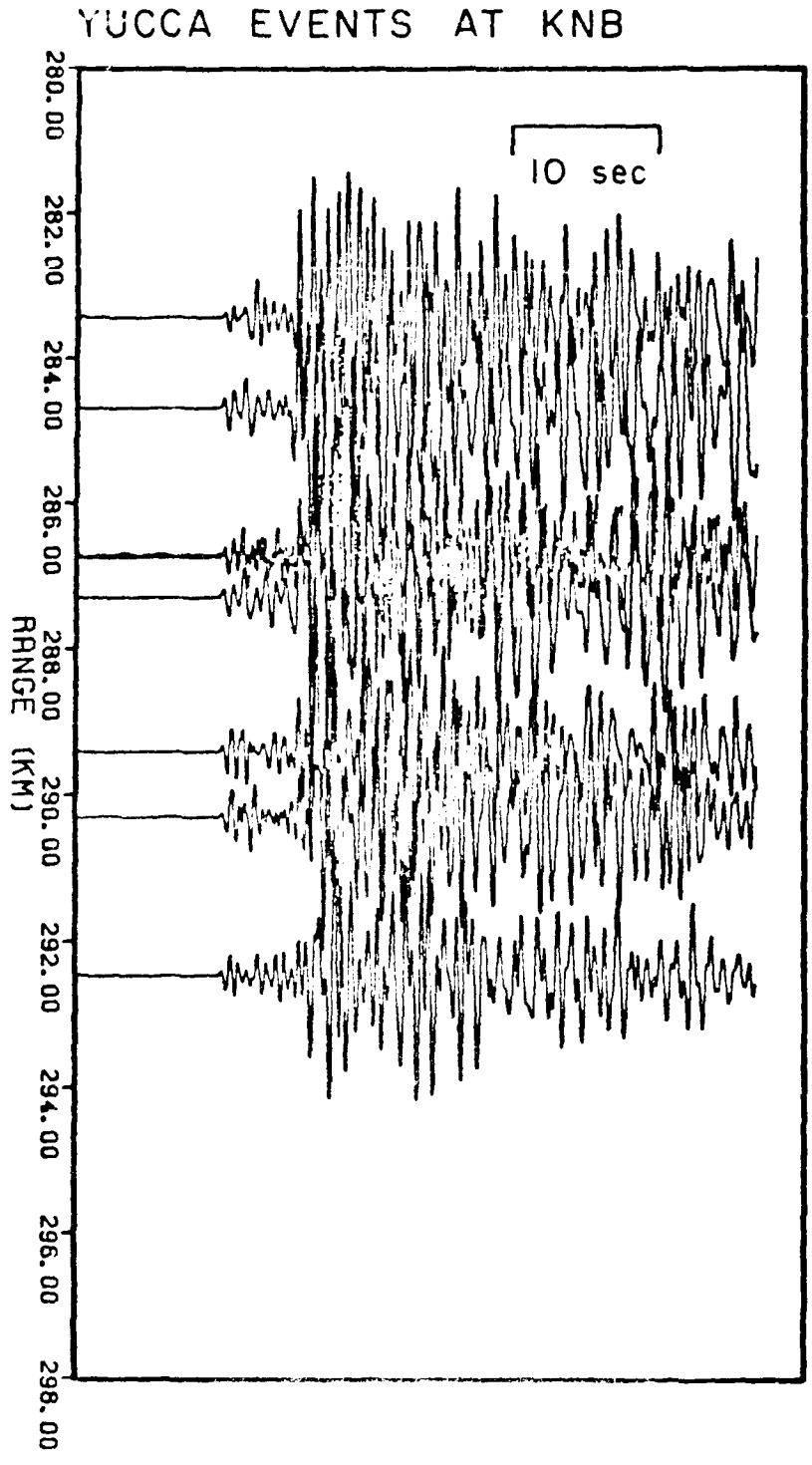

Figure A4. A seismic section of Yucca events observed at KNB.

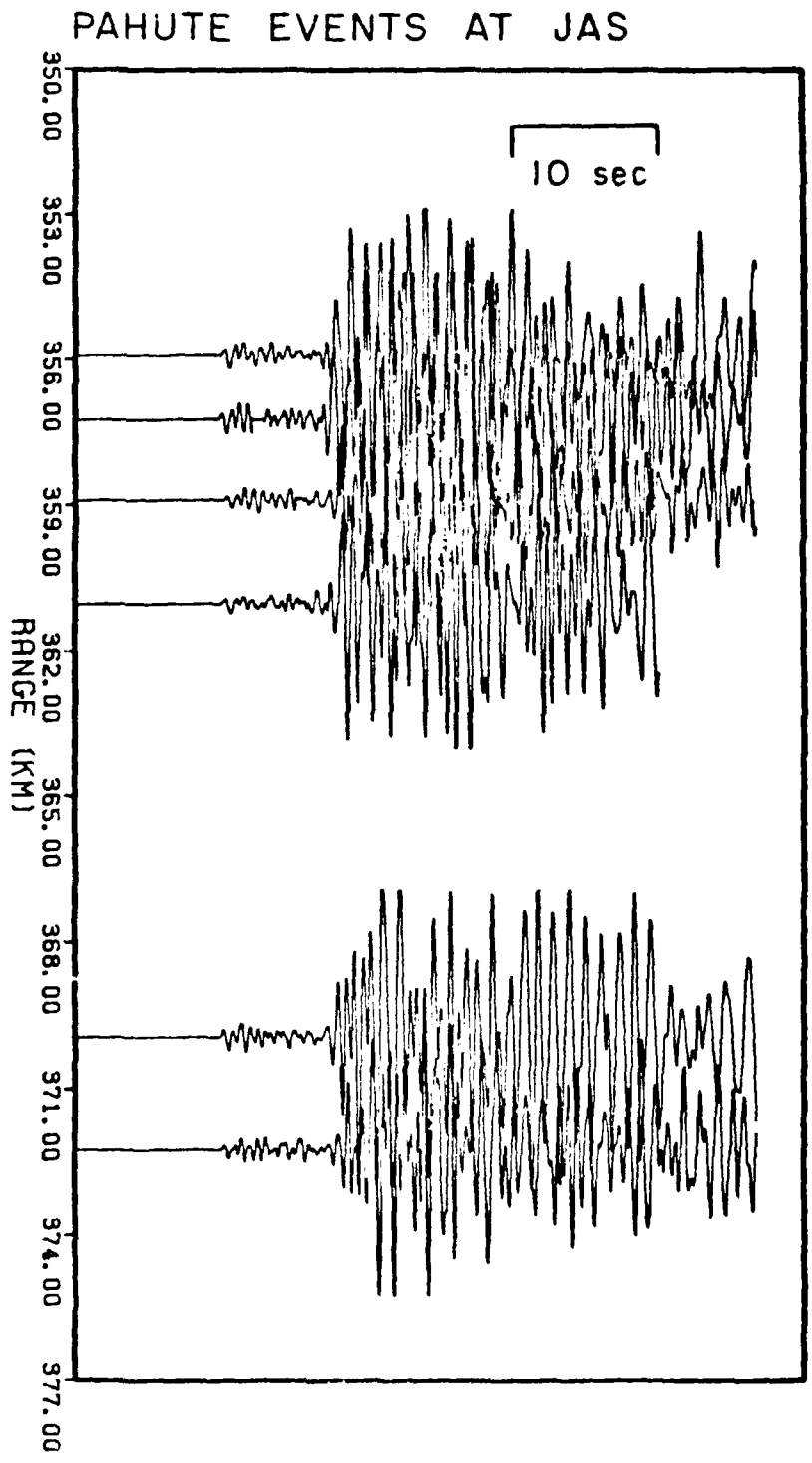

Figure A5. A seismic section of Pahute events observed at JAS.

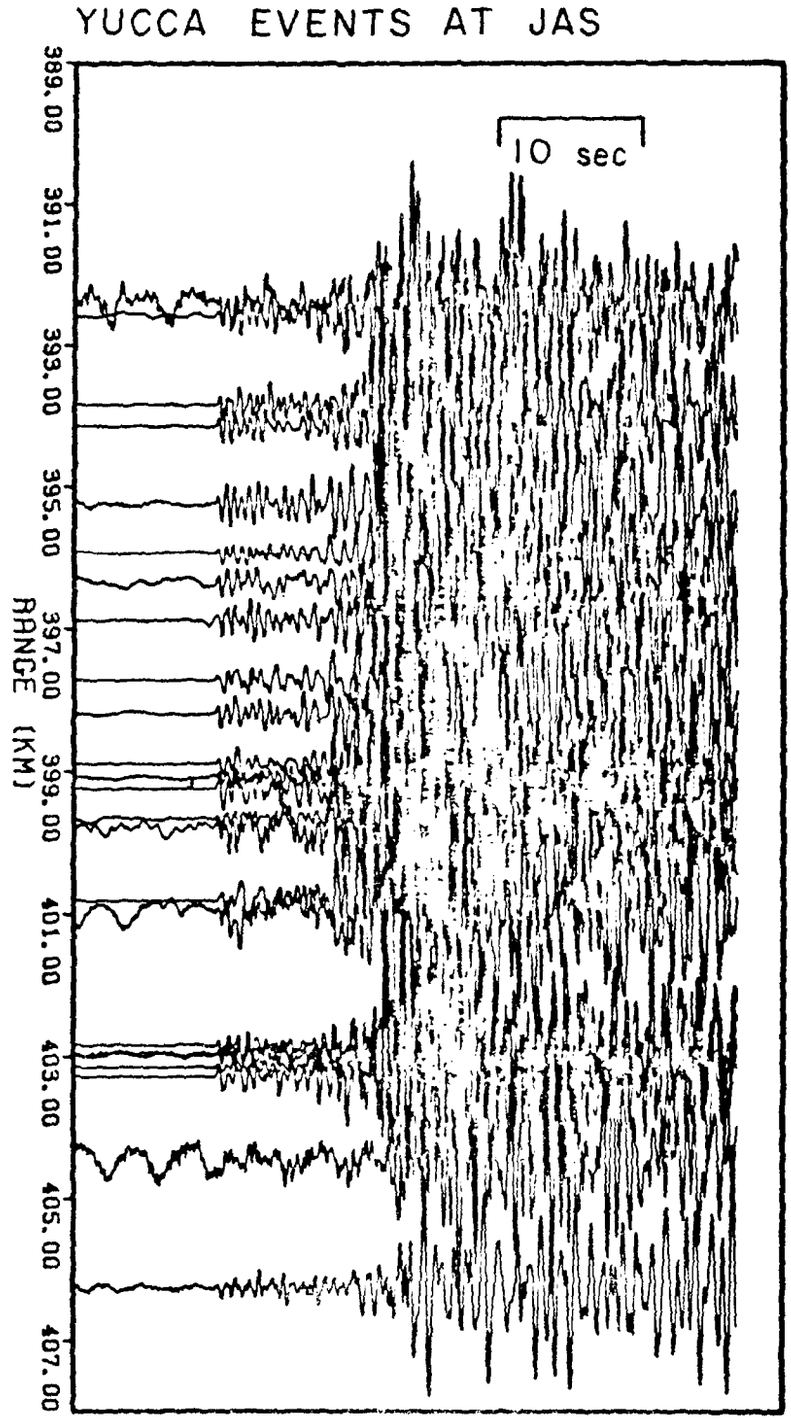

Figure A6. A seismic section of Yucca events observed at JAS.

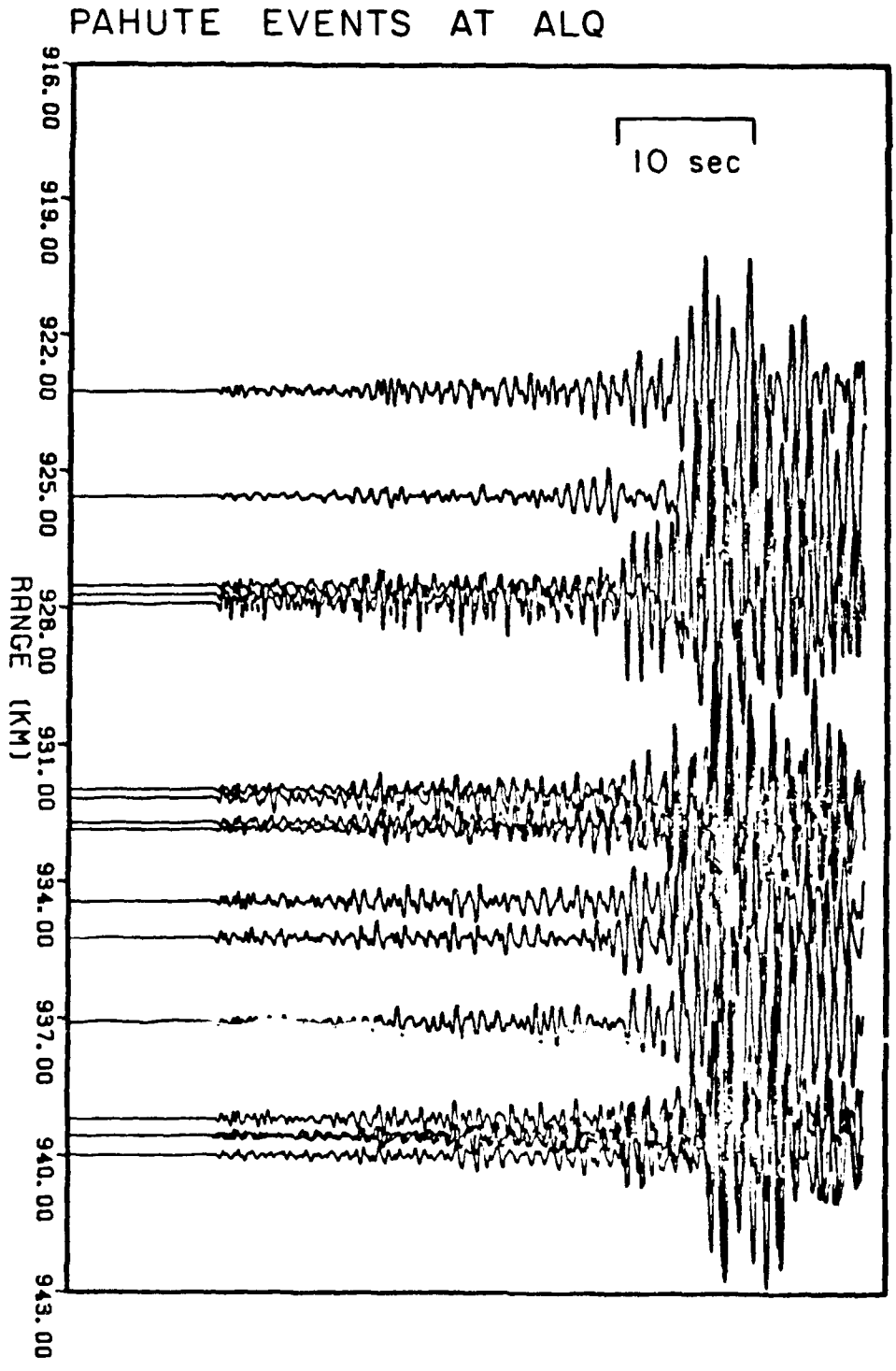

Figure A7. A seismic section of Pahute events observed at ALQ.

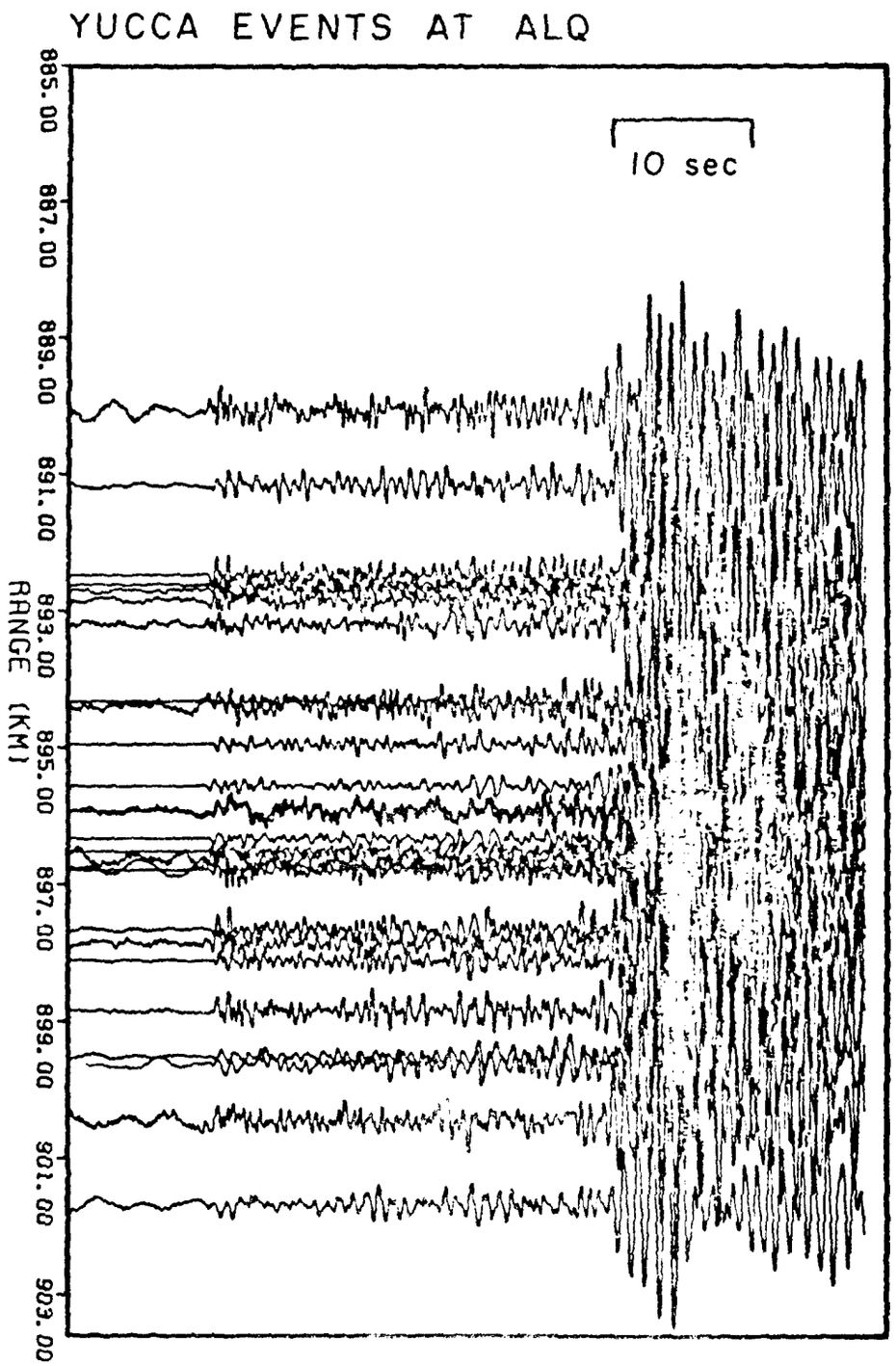

Figure A8. A seismic section of Yucca events observed at ALQ.

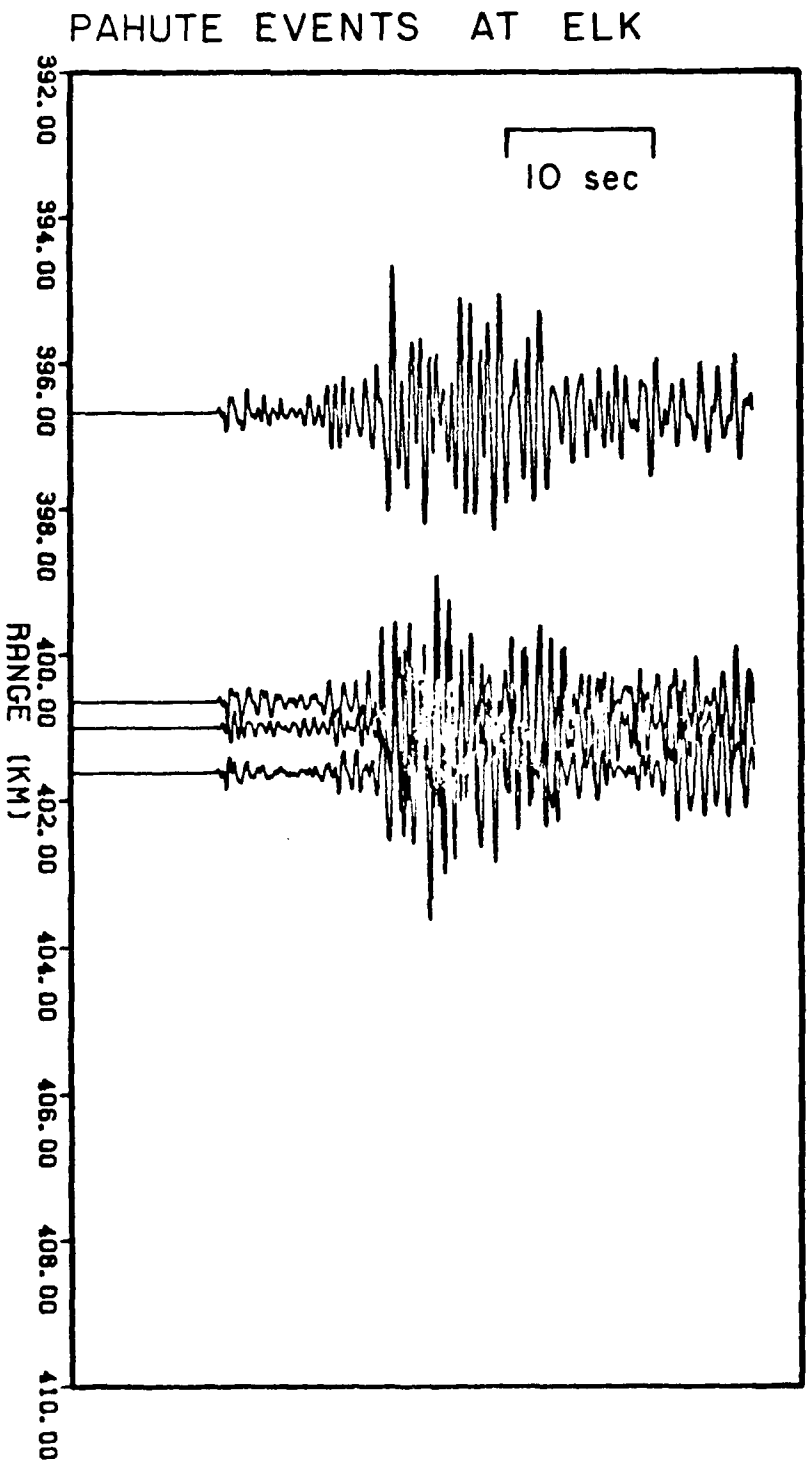

Figure A9. A seismic section of Pahute events observed at ELK.

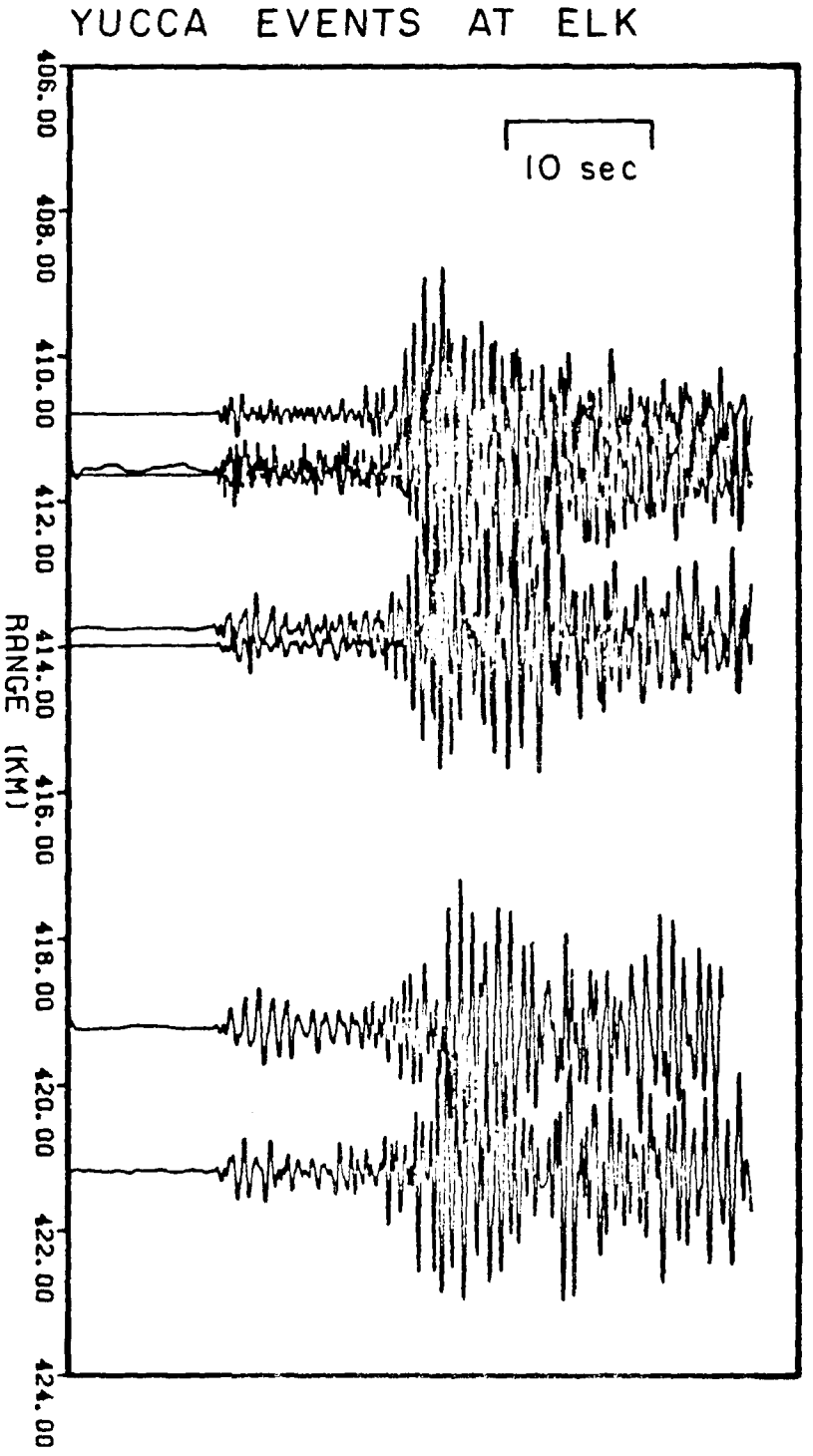

Figure A10. A seismic section of Yucca events observed at ELK.

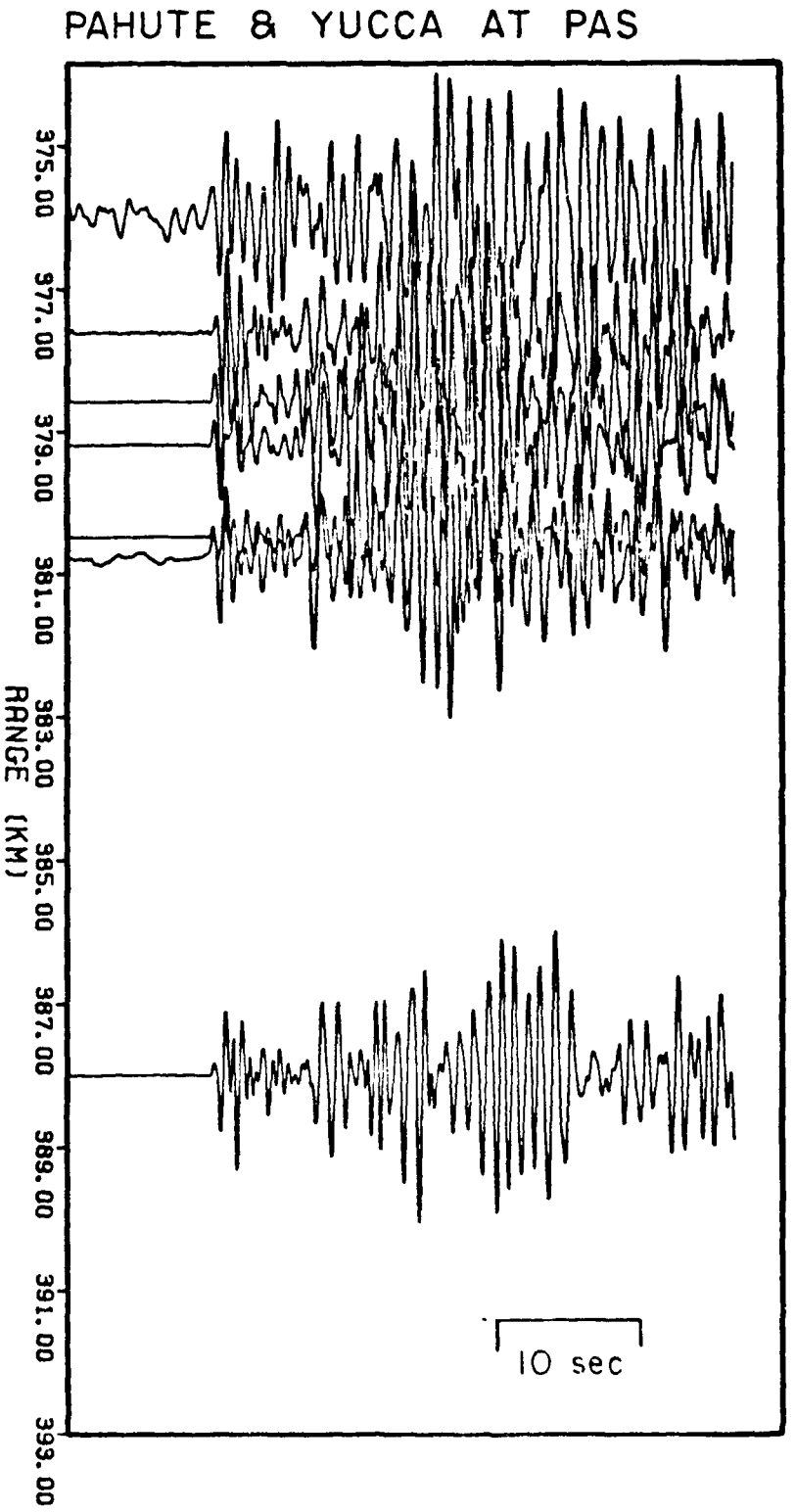

Figure A11 A seismic section of all available events observed at PAS.

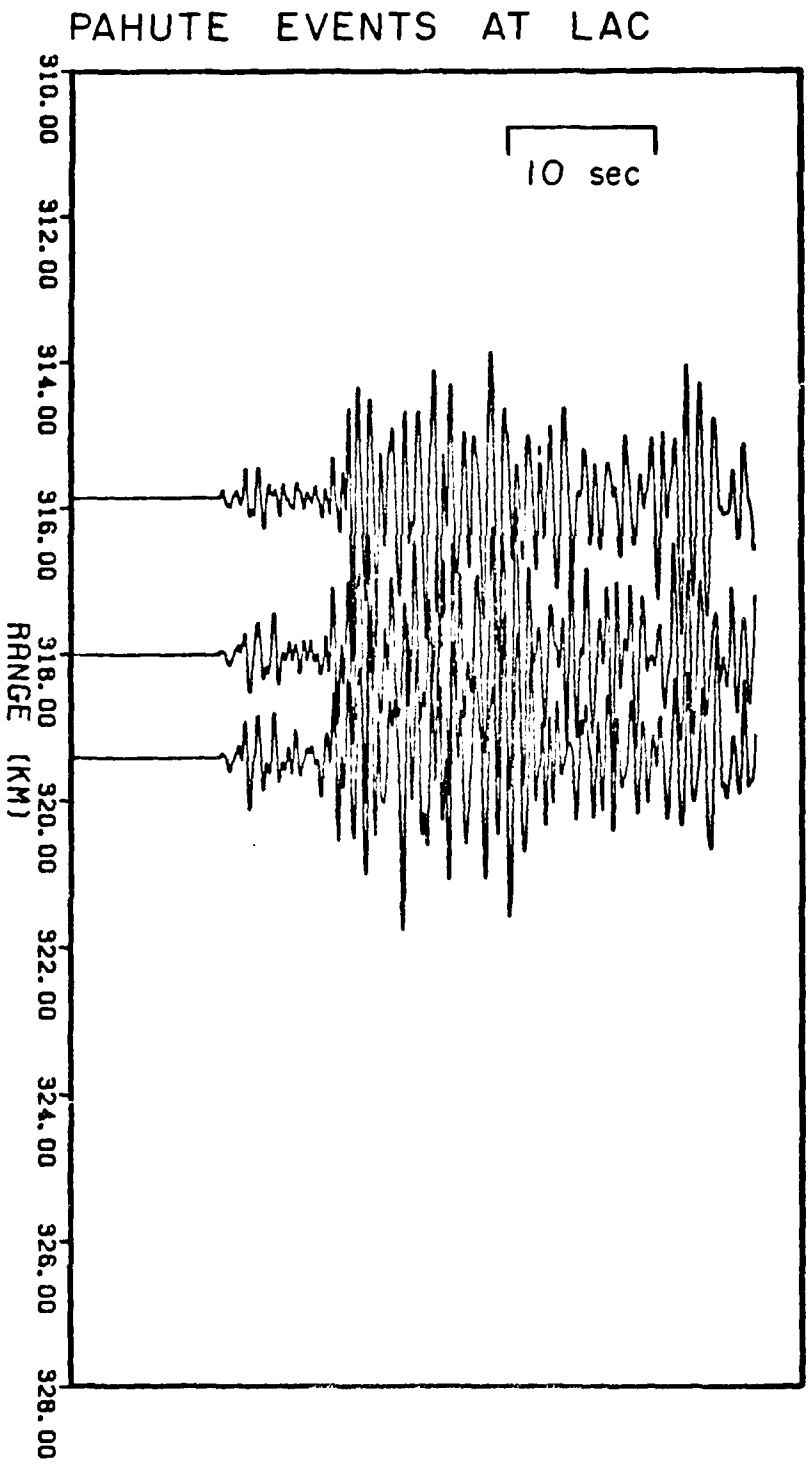

Figure A12. A seismic section of Pahute events observed at LAC.

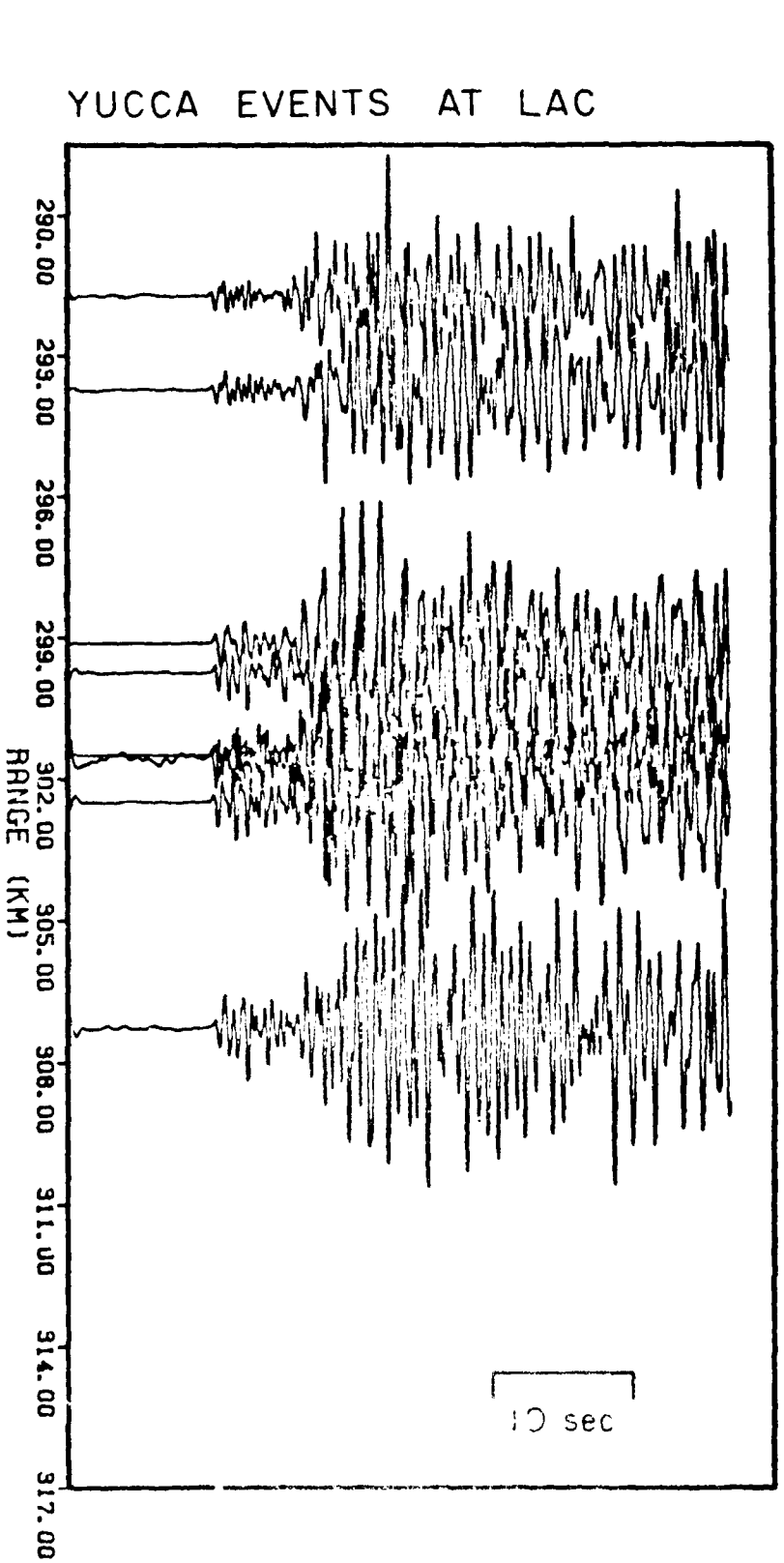

Figure A13. A seismic section of Yucca events observed at LAC.

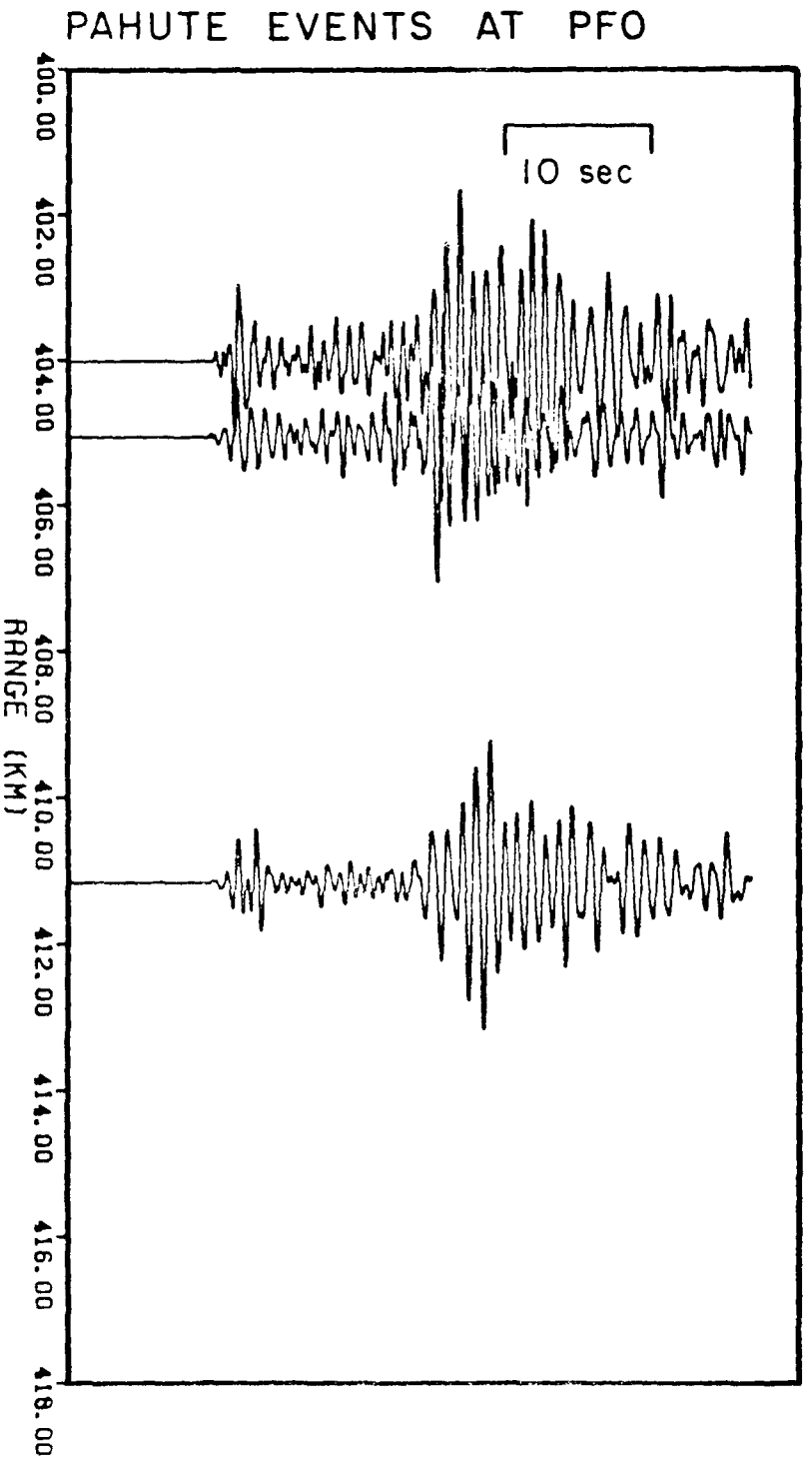

Figure A14. A seismic section of Pahute events observed at PFO.

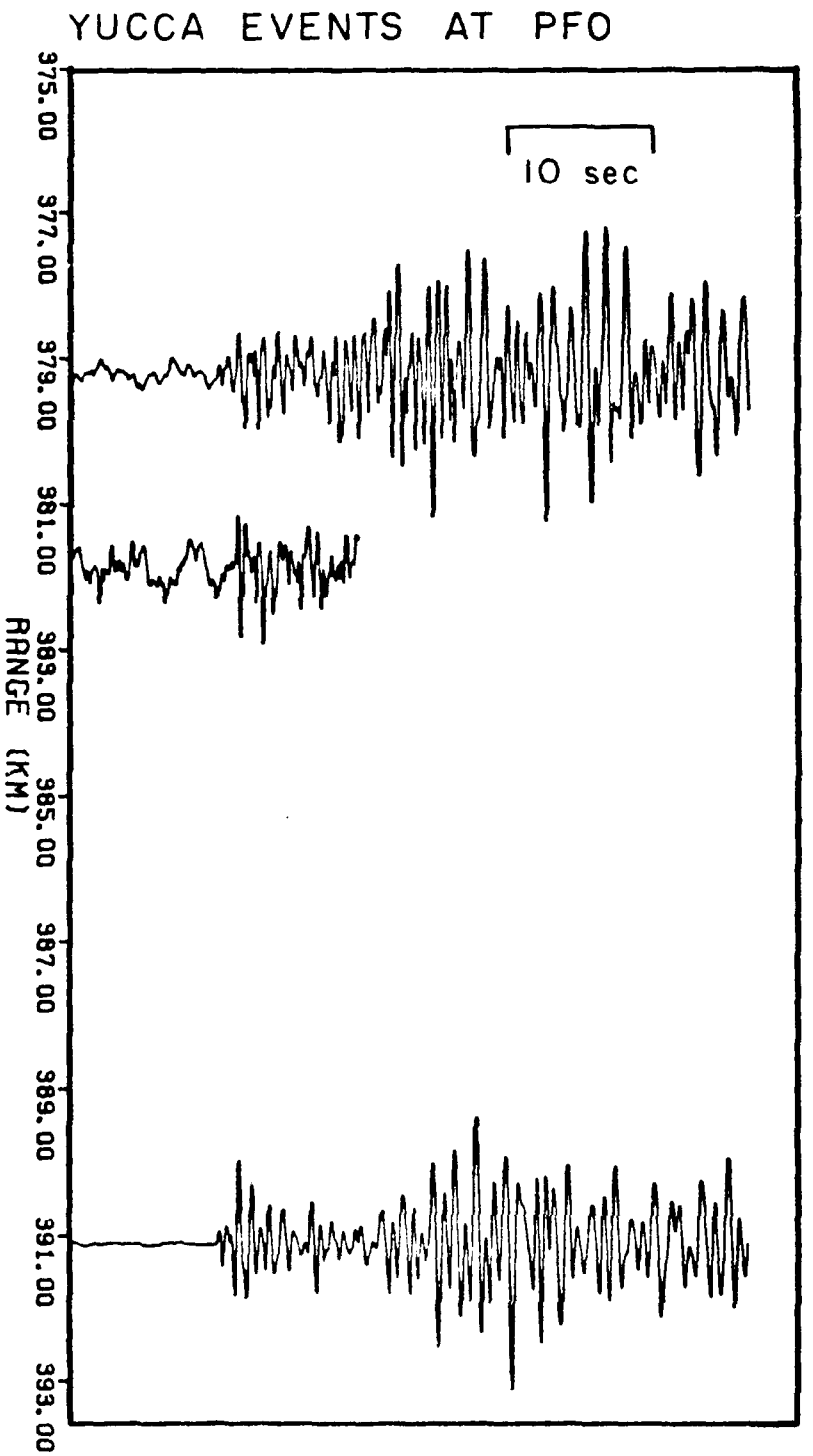

Figure A15. A seismic section of Yucca events observed at PFO.

CONTRACTORS (United States)

Professor Keiiti Aki
Center for Earth Sciences
University of Southern California
University Park
Los Angeles, CA 90089-0741

Professor Charles B. Archambeau
Cooperative Institute for Resch
in Environmental Sciences
University of Colorado
Boulder, CO 80309

Dr. Thomas C. Bache Jr.
Science Applications Int'l Corp.
10210 Campus Point Drive
San Diego, CA 92121 (2 copies)

Dr. Muawia Barazangi
Institute for the Study of the
Continent
SNEE Hall
Cornell University
Ithaca, NY 14853

Dr. Douglas R. Baumgardt
Signal Analysis & Systems Div.
ENSCO, Inc.
5400 Port Royal Road
Springfield, VA 22151-2388

Dr. Jonathan Berger
Institute of Geophysics and
Planetary Physics
Scripps Institution of Oceanography
A-025
University of California, San Diego
La Jolla, CA 92093

Dr. S. Bratt
Science Applications Int'l Corp.
10210 Campus Point Drive
San Diego, CA 92121

Dr. Lawrence J. Burdick
Woodward-Clyde Consultants
P.O. Box 93245
Pasadena, CA 91109-3245 (2 copies)

Professor Robert W. Clayton
Seismological Laboratory/Div. of
Geological & Planetary Sciences
California Institute of Technology
Pasadena, CA 91125

Dr Karl Coyner
N. E. Research, Inc.
76 Olcott Drive
White River Junction, VT 05001

Dr. Steven Day
Dept. of Geological Sciences
San Diego State U.
San Diego, CA 92182

Dr. Zoltan A. Der
ENSCO, Inc.
5400 Port Royal Road
Springfield, VA 22151-2388

Professor John Ferguson
Center for Lithospheric Studies
The University of Texas at Dallas
P.O. Box 830688
Richardson, TX 75083-0688

Professor Stanley Flatte'
Applied Sciences Building
University of California,
Santa Cruz, CA 95064

Dr. Alexander Florence
SRI International
333 Ravenswood Avenue
Menlo Park, CA 94025-3493

Professor Steven Grand
Department of Geology
245 Natural History Building
1301 West Green Street
Urbana, IL 61801

Dr. Henry L. Gray
Associate Dean of Dedman College
Department of Statistical Sciences
Southern Methodist University
Dallas, TX 75275

Professor Roy Greenfield
Geosciences Department
403 Deike Building
The Pennsylvania State University
University Park, PA 16802

Professor David G. Harkrider
Seismological Laboratory
Div of Geological & Planetary Sciences
California Institute of Technology
Pasadena, CA 91125

Dr. Vernon F. Cormier
Department of Geology & Geophysics
U-45, Room 207
The University of Conneticut
Storrs, Connecticut 06268

Professor Eugene Herrin
Institute for the Study of Earth
and Man/Geophysical Laboratory
Southern Methodist University
Dallas, TX 75275

Professor Robert B. Herrmann
Department of Earth & Atmospheric
Sciences
Saint Louis University
Saint Louis, MO 63156

Professor Bryan Isacks
Cornell University
Dept of Geological Sciences
SNEE Hall
Ithaca, NY 14850

Professor Lane R. Johnson
Seismographic Station
University of California
Berkeley, CA 94720

Professor Thomas H. Jordan
Department of Earth, Atmospheric
and Planetary Sciences
Mass Institute of Technology
Cambridge, MA 02139

Dr. Alan Kafka
Department of Geology &
Geophysics
Boston College
Chestnut Hill, MA 02167

Professor Leon Knopoff
University of California
Institute of Geophysics
& Planetary Physics
Los Angeles, CA 90024

Professor Charles A. Langston
Geosciences Department
403 Deike Building
The Pennsylvania State University
University Park, PA 16802

Professor Donald V. Helmberger
Seismological Laboratory
Div of Geological & Planetary Sciences
California Institute of Technology
Pasadena, CA 91125

Dr. Gary McCartor
Mission Research Corp.
735 State Street
P.O. Drawer 719
Santa Barbara, CA 93102 (2 copies)

Professor Thomas V. McEvilly
Seismographic Station
University of California
Berkeley, CA 94720

Dr. Keith L. McLaughlin
S-CUBED,
A Division of Maxwell Laboratory
P.O. Box 1620
La Jolla, CA 92038-1620

Professor William Menke
Lamont-Doherty Geological Observatory
of Columbia University
Palisades, NY 10964

Professor Brian J. Mitchell
Department of Earth & Atmospheric
Sciences
Saint Louis University
Saint Louis, MO 63156

Mr. Jack Murphy
S-CUBED
A Division of Maxwell Laboratory
11800 Sunrise Valley Drive
Suite 1212
Reston, VA 22091 (2 copies)

Professor J. A. Orcutt
Institute of Geophysics and Planetary
Physics, A-205
Scripps Institute of Oceanography
Univ. of California, San Diego
La Jolla, CA 92093

Professor Keith Priestley
University of Nevada
Mackay School of Mines
Reno, NV 89557

Professor Thorne Lay
Department of Geological Sciences
1006 C.C. Little Building
University of Michigan
Ann Arbor, MI 48109-1063

Dr. Randolph Martin III
New England Research, Inc.
76 Olcott Drive
White River Junction, VT 05001

Dr. Alan S. Ryall, Jr.
Center of Seismic Studies
1300 North 17th Street
Suite 1450
Arlington, VA 22209-2308 (4 copies)

Professor Charles G. Sammis
Center for Earth Sciences
University of Southern California
University Park
Los Angeles, CA 90089-0741

Professor Christopher H. Scholz
Geological Sciences
Lamont-Doherty Geological Observatory
Palisades, NY 10964

Dr. Jeffrey L. Stevens
S-CUBED,
A Division of Maxwell Laboratory
P.O. Box 1620
La Jolla, CA 92038-1620

Professor Brian Stump
Institute for the Study of Earth & Man
Geophysical Laboratory
Southern Methodist University
Dallas, TX 75275

Professor Ta-liang Teng
Center for Earth Sciences
University of Southern California
University Park
Los Angeles, CA 90089-0741

Professor Paul G. Richards
Lamont-Doherty Geological
Observatory of Columbia Univ.
Palisades, NY 10964

Wilmer Rivers
Teledyne Geotech
314 Montgomery Street
Alexandria, VA 22314

Dr. Clifford Thurber
State University of New York at
Stony Brooks
Dept of Earth and Space Sciences
Stony Brook, NY 11794-2100

Professor M. Nafi Toksoz
Earth Resources Lab
Dept of Earth, Atmospheric and
Planetary Sciences
Massachusetts Institute of Technology
42 Carleton Street
Cambridge, MA 02142

Professor Terry C. Wallace
Department of Geosciences
Building #77
University of Arizona
Tucson, AZ 85721

Weidlinger Associates
ATTN: Dr. Gregory Wojcik
4410 El Camino Real, Suite 110
Los Altos, CA 94022

Professor Francis T. Wu
Department of Geological Sciences
State University of New York
at Binghamton
Vestal, NY 13901

OTHERS (United States)

Dr. Monem Abdel-Gawad
Rockwell Internat'l Science Center
1049 Camino Dos Rios
Thousand Oaks, CA 91360

Professor Shelton S. Alexander
Geosciences Department
403 Deike Building
The Pennsylvania State University
University Park, PA 16802

Dr. Ralph Archuleta
Department of Geological
Sciences
Univ. of California at
Santa Barbara
Santa Barbara, CA

J. Barker
Department of Geological Sciences
State University of New York
at Binghamton
Vestal, NY 13901

Mr. William J. Best
907 Westwood Drive
Vienna, VA 22180

Dr. N. Biswas
Geophysical Institute
University of Alaska
Fairbanks, AK 99701

Dr. G. A. Bollinger
Department of Geological Sciences
Virginia Polytechnical Institute
21044 Derring Hall
Blacksburg, VA 24061

Dr. James Bulau
Rockwell Int'l Science Center
1049 Camino Dos Rios
P.O. Box 1085
Thousand Oaks, CA 91360

Mr. Roy Burger
1221 Serry Rd.
Schenectady, NY 12309

Dr. Robert Burridge
Schlumberger-Doll Resch Ctr.
Old Quarry Road
Ridgefield, CT 06877

Science Horizons, Inc.
ATTN: Dr. Theodore Cherry
710 Encinitas Blvd., Suite 101
Encinitas, CA 92024 (2 copies)

Professor Jon F. Claerbout
Professor Amos Nur
Dept. of Geophysics
Stanford University
Stanford, CA 94305 (2 copies)

Dr. Anton W. Dainty
AFGL/LWH
Hanscom AFB, MA 01731

Professor Adam Dziewonski
Hoffman Laboratory
Harvard University
20 Oxford St.
Cambridge, MA 02138

Professor John Ebel
Dept of Geology & Geophysics
Boston College
Chestnut Hill, MA 02167

Dr. Donald Forsyth
Dept. of Geological Sciences
Brown University
Providence, RI 02912

Dr. Anthony Gangi
Texas A&M University
Department of Geophysics
College Station, TX 77843

Dr. Freeman Gilbert
Institute of Geophysics &
Planetary Physics
Univ. of California, San Diego
P.O. Box 109
La Jolla, CA 92037

Mr. Edward Giller
Pacific Seirra Research Corp.
1401 Wilson Boulevard
Arlington, VA 22209

Dr. Jeffrey W. Given
Sierra Geophysics
11255 Kirkland Way
Kirkland, WA 98033

Rong Song Jih
Teledyne Geotech
314 Montgomery Street
Alexandria, Virginia 22314

Professor F.K. Lamb
University of Illinois at
Urbana-Champaign
Department of Physics
1110 West Green Street
Urbana, IL 61801

Dr. Arthur Lerner-Lam
Lamont-Doherty Geological Observatory
of Columbia University
Palisades, NY 10964

Dr. L. Timothy Long
School of Geophysical Sciences
Georgia Institute of Technology
Atlanta, GA 30332

Dr. Peter Malin
University of California at Santa Barbara
Institute for Central Studies
Santa Barbara, CA 93106

Dr. George R. Mellman
Sierra Geophysics
11255 Kirkland Way
Kirkland, WA 98033

Dr. Bernard Minster
Institute of Geophysics and Planetary
Physics, A-205
Scripps Institute of Oceanography
Univ. of California, San Diego
La Jolla, CA 92093

Professor John Nabelek
College of Oceanography
Oregon State University
Corvallis, OR 97331

Dr. Geza Nagy
U. California, San Diego
Dept of Ames, M.S. B-010
La Jolla, CA 92093

Dr. Jack Oliver
Department of Geology
Cornell University
Ithaca, NY 14850

Dr. Robert Phinney/Dr. F.A. Dahlen
Dept of Geological
Geophysical Sci. University
Princeton University
Princeton, NJ 08540 (2 copies)

RADIX Systems, Inc.
Attn: Dr. Jay Pulli
2 Taft Court, Suite 203
Rockville, Maryland 20850

Dr. Norton Rimer
S-CUBED
A Division of Maxwell Laboratory
P.O. 1620
La Jolla, CA 92038-1620

Professor Larry J. Ruff
Department of Geological Sciences
1006 C.C. Little Building
University of Michigan
Ann Arbor, MI 48109-1063

Dr. Richard Sailor
TASC Inc.
55 Walkers Brook Drive
Reading, MA 01867

Thomas J. Sereno, Jr.
Service Application Int'l Corp.
10210 Campus Point Drive
San Diego, CA 92121

Dr. David G. Simpson
Lamont-Doherty Geological Observ.
of Columbia University
Palisades, NY 10964

Dr. Bob Smith
Department of Geophysics
University of Utah
1400 East 2nd South
Salt Lake City, UT 84112

Dr. S. W. Smith
Geophysics Program
University of Washington
Seattle, WA 98195

Dr. Stewart Smith
IRIS Inc.
1616 N. Fort Myer Drive
Suite 1440
Arlington, VA 22209

Rondout Associates
ATTN: Dr. George Sutton,
Dr. Jerry Carter, Dr. Paul Pomeroy
P.O. Box 224
Stone Ridge, NY 12484 (4 copies)

Dr. L. Sykes
Lamont Doherty Geological Observ.
Columbia University
Palisades, NY 10964

Dr. Pradeep Talwani
Department of Geological Sciences
University of South Carolina
Columbia, SC 29208

Dr. R. B. Tittmann
Rockwell International Science Center
1049 Camino Dos Rios
P.O. Box 1085
Thousand Oaks, CA 91360

Professor John H. Woodhouse
Hoffman Laboratory
Harvard University
20 Oxford St.
Cambridge, MA 02138

Dr. Gregory B. Young
ENSCO, Inc.
5400 Port Royal Road
Springfield, VA 22151-2388

Dr. Peter Basham
Earth Physics Branch
Geological Survey of Canada
1 Observatory Crescent
Ottawa, Ontario
CANADA K1A 0Y3

Dr. Eduard Berg
Institute of Geophysics
University of Hawaii
Honolulu, HI 96822

Dr. Michel Bouchon - Universite
Scientifique et Medicale de Grenob
Lab de Geophysique - Interne et
Tectonophysique - I.R.I.G.M-B.P.
38402 St. Martin D'Heres
Cedex FRANCE

Dr. Hilmar Bungum/NTNF/NORSAR
P.O. Box 51
Norwegian Council of Science,
Industry and Research, NORSAR
N-2007 Kjeller, NORWAY

Dr. Michel Campillo
I.R.I.G.M.-B.P. 68
38402 St. Martin D'Heres
Cedex, FRANCE

Dr. Kin-Yip Chun
Geophysics Division
Physics Department
University of Toronto
Ontario, CANADA M5S 1A7

Dr. Alan Douglas
Ministry of Defense
Blacknest, Brimpton,
Reading RG7-4RS
UNITED KINGDOM

Dr. Manfred Henger
Fed. Inst. For Geosciences & Nat'l Res.
Postfach 510153
D-3000 Hannover 51
FEDERAL REPUBLIC OF GERMANY

Dr. E. Husebye
NTNF/NORSAR
P.O. Box 51
N-2007 Kjeller, NORWAY

Ms. Eva Johannisson
Senior Research Officer
National Defense Research Inst.
P.O. Box 27322
S-102 54 Stockholm
SWEDEN

Tormod Kvaerna
NTNF/NORSAR
P.O. Box 51
N-2007 Kjeller, NORWAY

Mr. Peter Marshall, Procurement
Executive, Ministry of Defense
Blacknest, Brimpton,
Reading FG7-4RS
UNITED KINGDOM (3 copies)

Dr. Ben Menaheim
Weizman Institute of Science
Rehovot, ISRAEL 951729

Dr. Svein Mykkeltveit
NTNF/NORSAR
P.O. Box 51
N-2007 Kjeller, NORWAY (3 copies)

Dr. Robert North
Geophysics Division
Geological Survey of Canada
1 Observatory crescent
Ottawa, Ontario
CANADA, K1A 0Y3

Dr. Frode Ringdal
NTNF/NORSAR
P.O. Box 51
N-2007 Kjeller, NORWAY

Dr. Jorg Schlittenhardt
Federal Inst. for Geosciences & Nat'l Res.
Postfach 510153
D-3000 Hannover 51
FEDERAL REPUBLIC OF GERMANY

University of Hawaii
Institute of Geophysics
ATTN: Dr. Daniel Walker
Honolulu, HI 96822

FOREIGN CONTRACTORS

Dr. Ramon Cabre, S.J.
Observatorio San Calixto
Casilla 5939
La Paz Bolvia

Professor Peter Harjes
Institute for Geophysik
Rhur University/Bochum
P.O. Box 102148, 4630 Bochum 1
FEDERAL REPUBLIC OF GERMANY

Professor Brian L.N. Kennett
Research School of Earth Sciences
Institute of Advanced Studies
G.P.O. Box 4
Canberra 2601
AUSTRALIA

Dr. B. Massinon
Societe Radiomana
27, Rue Claude Bernard
7,005, Paris, FRANCE (2 copies)

Dr. Pierre Mechler
Societe Radiomana
27, Rue Claude Bernard
75005, Paris, FRANCE

GOVERNMENT

Dr. Ralph Alewine III
DARPA/NMRO
1400 Wilson Boulevard
Arlington, VA 22209-2308

Dr. Robert Blandford
DARPA/NMRO
1400 Wilson Boulevard
Arlington, VA 22209-2308

Sandia National Laboratory
ATTN: Dr. H. B. Durham
Albuquerque, NM 87185

Dr. Jack Evernden
USGS-Earthquake Studies
345 Middlefield Road
Menlo Park, CA 94025

U.S. Geological Survey
ATTN: Dr. T. Hanks
Nat'l Earthquake Resch Center
345 Middlefield Road
Menlo Park, CA 94025

Dr. James Hannon
Lawrence Livermore Nat'l Lab.
P.O. Box 808
Livermore, CA 94550

Paul Johnson
ESS-4, Mail Stop J979
Los Alamos National Laboratory
Los Alamos, NM 87545

Ms. Ann Kerr
DARPA/NMRO
1400 Wilson Boulevard
Arlington, VA 22209-2308

Dr. Max Koontz
US Dept of Energy/DP 5
Forrestal Building
1000 Independence Ave.
Washington, D.C. 20585

Dr. W. H. K. Lee
USGS
Office of Earthquakes, Volcanoes,
& Engineering
Branch of Seismology
345 Middlefield Rd
Menlo Park, CA 94025

Dr. William Leith
USGS
Mail Stop 928
Reston, VA 22092

Dr. Richard Lewis
Dir. Earthquake Engineering and
Geophysics
U.S. Army Corps of Engineers
Box 631
Vicksburg, MS 39180

Dr. Robert Masse'
Box 25046, Mail Stop 967
Denver Federal Center
Denver, Colorado 80225

Richard Morrow
ACDA/VI
Room 5741
320 21st Street N.W.
Washington, D.C. 20451

Dr. Keith K. Nakanishi
Lawrence Livermore National Lab
P.O. Box 808, L-205
Livermore, CA 94550 (2 copies)

Dr. Carl Newton
Los Alamos National Lab.
P.O. Box 1663
Mail Stop C335, Group E553
Los Alamos, NM 87545

Dr. Kenneth H. Olsen
Los Alamos Scientific Lab.
Post Office Box 1663
Los Alamos, NM 87545

Howard J. Patton
Lawrence Livermore National
Laboratory
P.O. Box 808, L-205
Livermore, CA 94550

Mr. Chris Paine
Office of Senator Kennedy
SR 315
United States Senate
Washington, D.C. 20510

AFOSR/NP
ATTN: Colonel Jerry J. Perrizo
Bldg 410
Bolling AFB, Wash D.C. 20332-6448

HQ AFTAC/TT
Attn: Dr. Frank F. Pilotte
Patrick AFB, Florida 32925-6001

Mr. Jack Rachlin
USGS - Geology, Rm 3 C136
Mail Stop 928 National Center
Reston, VA 22092

Robert Reinke
AFWL/NTESG
Kirtland AFB, NM 87117-6008

HQ AFTAC/TGR
Attn: Dr. George H. Rothe
Patrick AFB, Florida 32925-6001

Donald L. Springer
Lawrence Livermore National Laboratory
P.O. Box 808, L-205
Livermore, CA 94550

Dr. Lawrence Turnbull
OSWR/NED
Central Intelligence Agency
CIA, Room 5G48
Washington, D.C. 20505

Dr. Thomas Weaver
Los Alamos National Laboratory
P.O. Box 1663
MS C335
Los Alamos, NM 87545

AFGL/SULL
Research Library
Hanscom AFB, MA 01731-5000 (2 copies)

Secretary of the Air Force (SAFRD)
Washington, DC 20330
Office of the Secretary Defense
DDR & E
Washington, DC 20330

DARPA/RMO/Security Office
1400 Wilson Blvd.
Arlington, VA 22209

HQ DNA
ATTN: Technical Library
Washington, DC 20305

AFGL/XO
Hanscom AFB, MA 01731-5000

AFGL/LW
Hanscom AFB, MA 01731-5000

DARPA/PM
1400 Wilson Boulevard
Arlington, VA 22209

Defense Technical
Information Center
Cameron Station
Alexandria, VA 22314
(5 copies)

Defense Intelligence Agency
Directorate for Scientific &
Technical Intelligence
Washington, D.C. 20301

Defense Nuclear Agency/SPSS
ATTN: Dr. Michael Shore
6801 Telegraph Road
Alexandria, VA 22310

AFTAC/CA (STINFO)
Patrick AFB, FL 32925-6001

Dr. Gregory van der Vink
Congress of the United States
Office of Technology Assessment
Washington, D.C. 20510

Mr. Alfred Lieberman
ACDA/VI-OA'State Department Building
Room 5726
320 - 21St Street, NW
Washington, D.C. 20451

TACTEC
Battelle Memorial Institute
505 King Avenue
Columbus, OH 43201 (Final report only)

DARPA/RMO/RETRIEVAL
1400 Wilson Boulevard
Arlington, VA 22209